INNATE IMMUNITY



# IRF1 cooperates with ISGF3 or GAF to form innate immune de novo enhancers in macrophages

**Carolina Chavez[1,2], Kelly Lin[2], Alexis Malveaux[2], Aleksandr Gorin[3], Stefanie Brizuela[4], Quen J. Cheng[3]*, Alexander Hoffmann[2]***

**Macrophages exposed to immune stimuli reprogram their epigenomes to alter their subsequent functions. Exposure to bacterial lipopolysaccharide (LPS) causes widespread nucleosome remodeling and the formation of thousands of de novo enhancers. We dissected the regulatory logic by which the network of interferon regulatory factors (IRFs) induces the opening of chromatin and the formation of de novo enhancers. We found that LPS-activated IRF3 mediated de novo enhancer formation indirectly by activating the type I interferon (IFN)–induced ISGF3. However, ISGF3 was generally needed to collaborate with IRF1, particularly where chromatin was less accessible. At these locations, IRF1 was required for the initial opening of chromatin, with ISGF3 extending accessibility and promoting the deposition of H3K4me1, marking poised enhancers. Because *IRF1* expression depends on the transcription factor NF-κB, which is activated in infected but not bystander cells, IRF-regulated enhancers required activation of both the IRF3 and NF-κB branches of the innate immune signaling network. However, type II IFN (IFN-γ), which is typically produced by T cells, may also induce *IRF1* expression through the STAT1 homodimer GAF. We showed that, upon IFN-γ stimulation, IRF1 was also responsible for opening inaccessible chromatin sites that could then be exploited by GAF to form de novo enhancers. Together, our results reveal how combinatorial logic gates of IRF1-ISGF3 or IRF1-GAF restrict immune epigenomic memory formation to macrophages exposed to pathogens or IFN-γ–secreting T cells but not bystander macrophages exposed transiently to type I IFN.**

## INTRODUCTION

Macrophages are key components of the innate immune system that adapt their functions to microenvironmental context and in response to prior exposure to cytokines or pathogen components (*1*). The latter has been described as innate immune memory resulting in trained immunity (*2*), expanding the well-established concepts of macrophage polarization (*3*) and endotoxin-induced tolerance (*4*). There are three broad mechanisms underlying innate immune training: stimulus-induced adaptation of signaling pathways (for example, through modulation of receptor expression or induction of positive or negative signal transducers) (*5*), metabolic reprogramming (*6*), or epigenetic reprogramming by the formation of de novo enhancers (*7*). Latent enhancers are chromatinized genomic regions that are opened in response to a specific stimulus to increase their accessibility. When they gain monomethylation of lysine-4 of histone H3 (H3K4me1), a marker of poised enhancers (*8*), they are considered de novo enhancers. Acetylation of lysine-27 of histone H3 (H3K27ac) indicates transcriptional activity and therefore marks active enhancers (*9*). The persistence of histone modifications even after removal of the initial activation suggests epigenetic immune memory that reprograms the macrophage's subsequent stimulus responses (*10*).

Lineage-determining transcription factors (LDTFs), such as PU.1, are critical for the establishment and maintenance of macrophage lineage–specific enhancers (*9*, *11*). In contrast, the formation of de novo enhancers in response to cytokines or pathogen-associated molecular patterns (PAMPs) is mediated by stimulus-dependent transcription factors (SDTFs), such as nuclear factor κB (NF-κB) (*8*, *12*–*14*). The underlying mechanisms of de novo enhancer formation involve two distinguishable phases. First, SDTFs bind to cognate sequences within nucleosomal DNA, which produces nucleosomal opening and increased chromatin accessibility within a matter of minutes, potentially in cooperation with chromatin-remodeling enzymes, such as SWI/SNF (SWItch/Sucrose Non-Fermentable), FACT (Facilitates Chromatin Transcription), and RNA polymerase II (RNA Pol II) (*12*, *15*). Second, SDTFs may contribute to the recruitment of LDTFs (for example, PU.1) to maintain open chromatin and chromatin-modifying enzymes to catalyze the deposition of H3K4me1 and H3K27ac within hours after stimulation (*8*, *11*, *12*).

Studies have shown that the formation of de novo enhancers is stimulus-specific (*8*, *14*). NF-κB opens chromatin (*14*, *16*) and induces hundreds of de novo enhancers but only when it is activated with nonoscillatory dynamics (*14*). This dynamic requirement ensures that enhancer formation is restricted to MyD88-mediated signals emanating from bacterial PAMPs, such as lipopolysaccharide (LPS; also known as endotoxin), but not paracrine tumor necrosis factor (TNF), which activates NF-κB with oscillatory dynamics. A second set of hundreds of de novo enhancers are associated with interferon-stimulated response elements (ISREs), the cognate motif for the family of interferon regulatory factors (IRFs). Of the nine IRF family members, IRF1, IRF3, and IRF9 (which is part of the ISGF3 complex) are relevant for stimulus responses in murine macrophage colony-stimulating factor (M-CSF)–differentiated bone marrow–derived macrophages (BMDMs) (*17*). A key impediment to dissecting the functional specificity of IRFs is their largely overlapping binding specificity for the ISRE GAAANNGAAACT and their interdependent activation mechanisms (*18*, *19*). Whereas the first PAMP-responsive IRF is IRF3, its induction of interferon-β (IFN-β) stimulates activation of the transcription factor ISGF3 (IRF9) through the interferon-α/β receptor (IFNAR), which dominates the subsequent gene expression response (*19*). However, which IRF family member is

[1]Molecular and Medical Pharmacology PhD Program, UCLA, Los Angeles, CA, USA. [2]Department of Microbiology, Immunology and Molecular Genetics, UCLA, Los Angeles, CA, USA. [3]Department of Medicine, David Geffen School of Medicine at UCLA, Los Angeles, CA, USA. [4]Molecular Biology PhD Program, UCLA, Los Angeles, CA, USA.
*Corresponding author. Email: quencheng@ucla.edu (Q.J.C.); ahoffmann@ucla.edu (A.H.)

responsible for the induction of ISRE-associated de novo enhancers is unknown.

Here, we combined a genetic approach with biochemical characterization of the IRF signaling network and epigenomic profiling to delineate the signaling roles of IRF family members in de novo enhancer formation during the innate immune response. We found that IRF3 acts directly only at a minority of de novo enhancers, but its major role is indirect through the induction of IFN-β induction and consequent ISGF3 activation. However, ISGF3 requires the coordinated function of IRF1, which is activated by NF-κB in cells responding to pathogen exposure. IRF1 is also induced by type II IFN, and in this context, it cooperates with IFN-γ–activated factor (GAF) to stimulate formation of de novo enhancers. We conclude that, although IRF1 is a versatile, chromatin-remodeling SDTF, it must function combinatorially with other SDTFs (ISGF3 or GAF) to ensure that long-lasting epigenome remodeling is restricted and does not occur in all cells that gain antiviral protection from paracrine type I IFN.

## RESULTS

### Many LPS-induced de novo enhancers are associated with an ISRE and type I IFN signaling

Our previous studies revealed that de novo enhancers induced by LPS in BMDMs and associated with ISRE motifs were abolished by the combined deficiency of IFNAR and IRF3 (*Ifnar*$^{-/-}$*Irf3*$^{-/-}$ BMDMs), which abrogates both IRF3 and ISGF3 activity (*14*). To dissect the contributions of IRF3 and ISGF3 in de novo enhancer formation (Fig. 1A), we stimulated BMDMs generated from wild-type (WT), *Irf3*$^{-/-}$*Ifnar*$^{-/-}$, *Ifnar*$^{-/-}$, and *Irf3*$^{-/-}$ mice with LPS (100 ng/ml) for 8 hours. We performed chromatin immunoprecipitation sequencing (ChIP-seq) with a validated antibody against H3K4me1 and identified 4800 de novo enhancer regions by applying a cutoff for the false discovery rate (FDR) of $< 0.05$ and for the $\log_2$ fold change (LFC) of $> 0.5$ of triplicate data upon stimulation of WT cells with LPS. More than 90% of these H3K4me1 regions were in intergenic and intronic regions, whereas a minority of locations were found in transcription start site (TSS) or exonic regions (fig. S1A). When considering knockout data, these 4800 de novo enhancers clustered into two major groups by unsupervised *k*-means clustering (Fig. 1B): Cluster 1 (C1) was enriched for the IRF DNA binding motif known as ISRE, whereas cluster 2 (C2) was enriched for NF-κB motifs. Consistent with our previous findings (*14*), we observed a substantial loss of C1 de novo ISRE enhancer formation in *Irf3*$^{-/-}$*Ifnar*$^{-/-}$ cells (Fig. 1B). Both *Ifnar*$^{-/-}$ and *Irf3*$^{-/-}$ single knockouts also showed deficiencies in the formation of C1 de novo ISRE enhancers (Fig. 1B), suggesting that both IRF3 and ISGF3 are required for the formation of ISRE enhancers.

To further characterize these de novo enhancers, we examined publicly available ChIP-seq datasets of H3K27ac, PU.1, and RNA

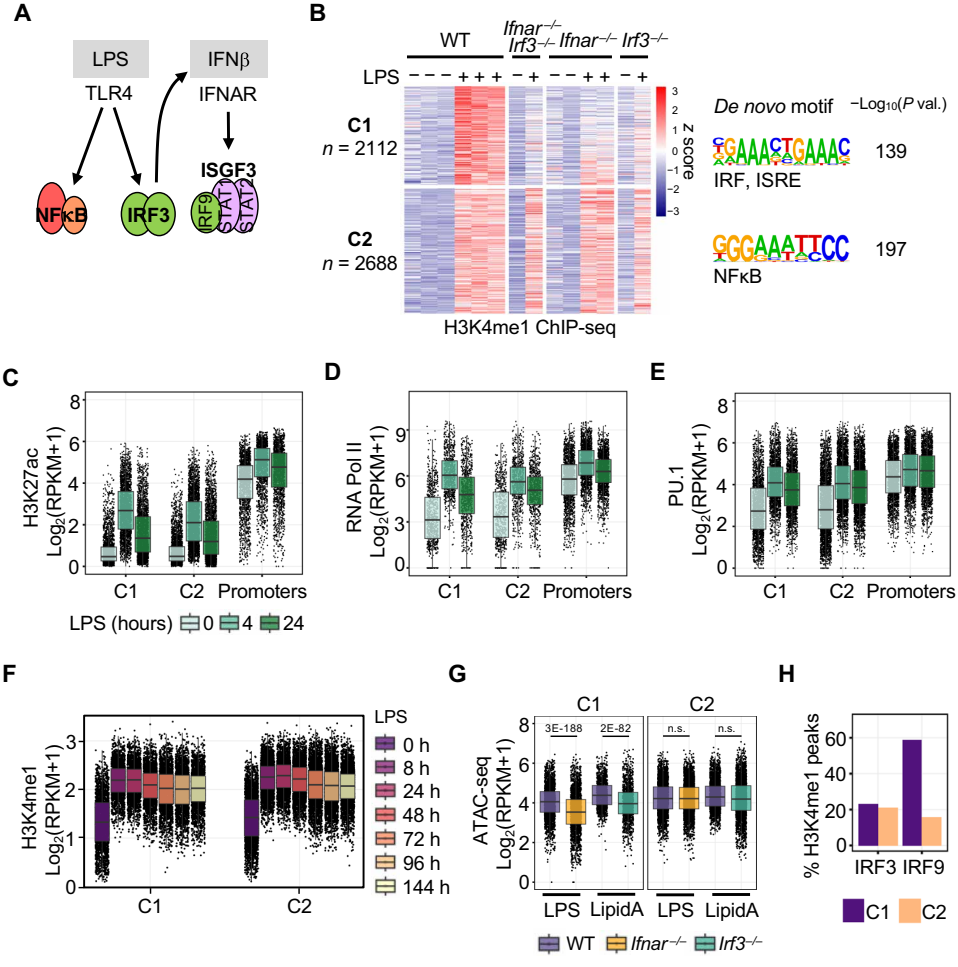


**Fig. 1. IRF3 and ISGF3 stimulate the formation of long-lasting de novo enhancers.** (**A**) Schematic of the LPS signaling network, including secondary ISGF3 activation by IFN-β. (**B**) Heatmap of the *z*-scored H3K4me1 ChIP-seq data for 4800 locations induced (LFC > 0.5, FDR < 0.05) by 8 hours of stimulation with LPS (100 ng/ml). Clusters generated by unsupervised *k*-means were subjected to de novo motif analysis. Right: The top enriched sequences. Each column represents a single mouse, with $n = 3$ WT mice. (**C** to **E**) Boxplots of the $\log_2$ RPKM normalized ChIP-seq data (GSE38377) for (C) H3K27ac, (D) RNA Pol II, and (E) PU.1 in the LPS-induced C1 or C2 de novo enhancers or promoter regions of LPS-inducible genes (LFC > 0.5). Data are from a single mouse per antibody. (**F**) Boxplots of the $\log_2$ RPKM normalized H3K4me1 ChIP-seq on different time intervals after removal of LPS after 8 hours of stimulation. Data are from a single mouse per time point. h, hours. (**G**) Boxplots of the $\log_2$ RPKM ATAC-seq signals at C1 or C2 enhancer locations in WT, *Ifnar*$^{-/-}$, and *Irf3*$^{-/-}$ (GSE234914) BMDMs treated for 3 hours with LPS or lipid A (100 ng/ml). Data are the average of two or three mice per condition. Statistical evaluation used the Wilcoxon signed-rank test for paired data. (**H**) Percentage of H3K4me1 peaks overlapping with the IRF3 (GSE67357) or IRF9 (GSE115435) ChIP-seq peaks on C1 or C2 enhancer locations. Data are from two mice per condition.

Pol II on LPS-stimulated BMDMs (*8*). We found that most de novo ISRE enhancers acquire the active enhancer mark H3K27ac at the 4-hour time point (Fig. 1C), but this signal is transient given that it decreases from a median $\log_2$ reads per kilobase per million mapped reads (RPKM) value of 2.7 at 4 hours to 1.4 at the 24-hour time point (Fig. 1C). Similar observations pertain to the NF-κB–regulated enhancers of cluster C2. In contrast, promoter regions of LPS-inducible genes (LFC > 0.5, at 8 hours) had median $\log_2$ RPKM values of 4.2 before stimulation (Fig. 1C), indicating that many promoters were primed in naïve macrophages. RNA Pol II occupancy at the basal state was higher in promoters (median $\log_2$ RPKM = 5.8) than C1 (median $\log_2$ RPKM = 3.1) or C2 (median $\log_2$ RPKM = 3.3) enhancers, but the enzyme was recruited to both IRF- and NF-κB–associated enhancers at 4 hours (Fig. 1D). We next examined the binding patterns of PU.1, the macrophage LDTF that establishes macrophage enhancers (*8*, *20*, *21*). We found that PU.1 binding was induced substantially at both the C1 and C2 enhancer locations within 4 hours of LPS stimulation and persisted for at least 24 hours (Fig. 1E). In contrast, PU.1 signals at promoters of LPS-inducible genes already high before stimulation and barely inducible. Together, these results suggest that, in contrast with LPS-inducible promoters that are primed with RNA Pol II, PU.1, and H3K27ac, latent de novo enhancer regions are in a more inactive state, from which they must be activated by stimulus-induced SDTFs that initiate chromatin remodeling.

To investigate the longevity of the IRF- and NF-κB–associated enhancers, we removed the LPS after an 8-hour stimulation and performed H3K4me1 ChIP-seq in a subsequent time course. Contrary to the transient H3K27ac epigenetic changes, the H3K4me1 marks remained largely unchanged for at least 6 days after stimulation in both the C1 and C2 de novo enhancers (Fig. 1F). Only 738 enhancers decreased more than 0.5 LFC, compared with 4062 enhancers that remained unchanged. We did not find a difference in sequence composition between these enhancers. The longer-lasting temporal dynamics of H3K4me1 suggests that these enhancers remain in a "poised" state that enables rapid activation in response to subsequent stimulation, consistent with previous findings (*7*, *8*, *14*).

Our results suggest that, in response to LPS exposure, the activation dynamics of de novo ISRE enhancers are similar to those previously described for NF-κB–associated enhancers and that both IRF3 and ISGF3 are required for their formation. To further address the relative contributions of IRF3 and ISGF3, we investigated their respective roles in opening chromatin at LPS-induced enhancer locations with an assay for transposase-accessible chromatin with sequencing (ATAC-seq) dataset from WT and *Ifnar*$^{-/-}$ BMDMs (LPS-treated) and WT and *Irf3*$^{-/-}$ BMDMs (lipid A–treated) (*16*). Knockouts of either factor (*Ifnar*$^{-/-}$ or *Irf3*$^{-/-}$) resulted in deficiency in chromatin accessibility within 2 hours of stimulation with LPS of C1 but not C2 enhancers (Fig. 1G). However, when we analyzed ChIP-seq datasets for IRF3 in lipid A–treated BMDMs (*22*) or for IRF9 in IFN-β–treated BMDMs (*23*), we found that, whereas IRF9 was frequently found on C1 de novo enhancers (58%), IRF3 binding to C1 and C2 enhancers was similarly low (~22%) (Fig. 1H). These results suggest that IRF3 may have not only direct but also indirect roles in de novo ISRE enhancer formation. An indirect role is also suggested by the observation that new protein synthesis is required for many ISRE-associated chromatin-opening events and that IRF3 is directly involved in a small number of locations (*16*).

## ISGF3 is required but not sufficient to form most ISRE de novo enhancers

We considered that IRF3 may indirectly generate de novo enhancers through IFN-β production that activates ISGF3. To further understand the interplay between IRF3 and ISGF3 activity, we performed Western blotting analysis of nuclear extracts from *Irf3*$^{-/-}$ BMDMs. We observed a deficiency in the activation of the ISGF3 subunits signal transducer and activator of transcription 1 (STAT1) and STAT2 in response to LPS (Fig. 2A), consistent with the role of IRF3 in IFN-β production (*24*). Thus, deficiencies in enhancer formation observed in IRF3-deficient cells may be due to defects in ISGF3 activation. To determine whether IRF3 was directly involved in enhancer formation, we rescued ISGF3 activation in *Irf3*$^{-/-}$ BMDMs by costimulating LPS-treated cells with IFN-β (0.3 or 10 U/ml) after 1 hour of the LPS stimulation time course (Fig. 2A). Costimulation with IFN-β at 10 U/ml resulted in similar amounts of nuclear pSTAT1 and pSTAT2 as those seen LPS-treated WT cells. We therefore performed H3K4me1 ChIP-seq with *Irf3*$^{-/-}$ BMDMs stimulated with LPS alone or with IFN-β (Fig. 2, B and C). We observed a 57% median increase in H3K4me1 signal in de novo ISRE enhancers with the addition of IFN-β ($P < 0.001$) (Fig. 2B) and a smaller difference in the NF-κB–regulated enhancers (Fig. 2C).

We further analyzed the data to distinguish between de novo enhancers on the basis of their involvement with IRF3 by classifying the C1 enhancers into three different groups based on WT-to-*Irf3*$^{-/-}$ LFC differences (WT/*Irf3*$^{-/-}$); C1.1 enhancers were deficient in *Irf3*$^{-/-}$ BMDMs and were not rescued by IFN-β (LFC > 0.5 in LPS and LFC > 0.5 in LPS + IFN-β); C1.2 enhancers were rescued by IFN-β (LFC > 0.5 in LPS and LFC < 0.5 in LPS + IFN-β); and C1.3 enhancers showed only a moderate decrease in *Irf3*$^{-/-}$ BMDMs (LFC < 0.5 in LPS) (Fig. 2D). Of the 1090 de novo enhancers substantially affected by IRF3 deficiency, we found that 870 were rescued by the addition of IFN-β (C1.2), whereas only 220 locations remained deficient in enhancer formation even in the presence of ISGF3 activation (C1.1) (Fig. 2E). These data indicate that the IRF3-ISGF3 axis plays an important role in the formation of enhancers, although a minority of regions may be regulated directly by IRF3.

To determine the regulatory control of chromatin opening, we examined ATAC-seq data from endotoxin-treated BMDMs (*16*). We observed that IRF3-regulated de novo enhancers (C1.1) were more defective in chromatin opening in *Irf3*$^{-/-}$ BMDMs than those that were rescued by IFN-β–induced ISGF3 (Fig. 2F). In the basal state of WT macrophages, C1.1 locations showed slightly less accessibility than C1.2 locations and statistically significantly less accessibility than C1.3 locations (fig. S1B). IRF3 binding after 2 hours of stimulation with lipid A was significantly greater at the IRF3-dependent locations (C1.1) than at the C1.2 or C1.3 enhancers (Fig. 2G). These results identify C1.1 locations as being directly IRF3-regulated.

However, because most C1 enhancers were dependent on ISGF3 and not IRF3, we asked whether ISGF3 alone was sufficient to stimulate the formation of these enhancers. We stimulated WT macrophages with IFN-β at a concentration that fully activates ISGF3 but not IRF3. We found that IFN-β had little effect on the C1.1 and C1.3 locations (median LFCs of 0.16 and 0.14, respectively) and had only a slightly greater effect on C1.2 locations (median LFC of 0.25) (Fig. 2H). In contrast, LPS induced C1.1 and C1.2 enhancers by about 1.0 median LFC. These results demonstrate that ISGF3 is necessary but not sufficient to produce most LPS-induced de novo ISRE enhancers.

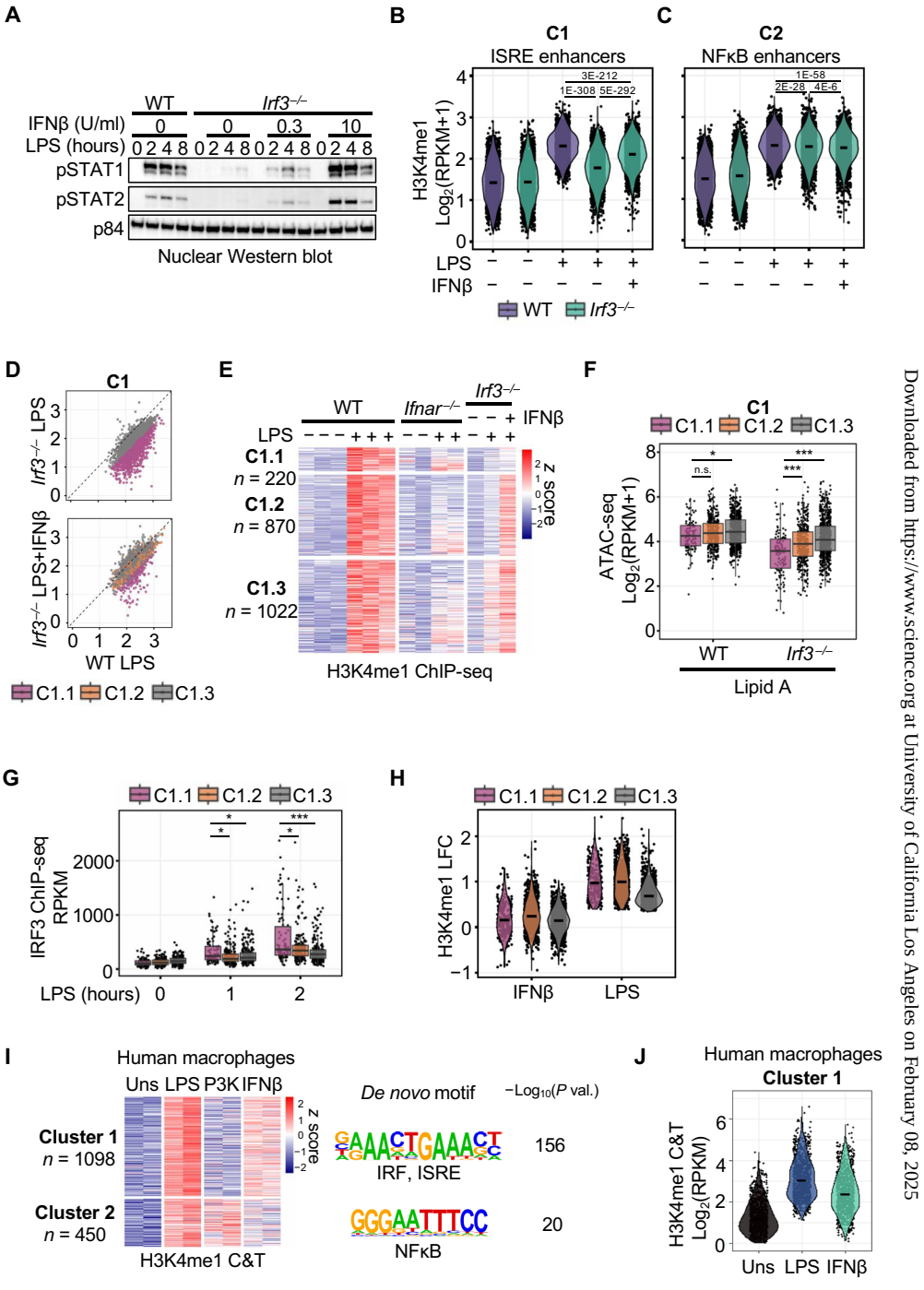


**Fig. 2. ISGF3 is required but is not sufficient to induce most ISRE enhancers.** (**A**) Western blotting analysis of pSTAT1, pSTAT2, and the loading control p84 in nuclear extracts from WT and *Irf3*$^{-/-}$ BMDMs stimulated with LPS, with the indicated addition of IFN-β at the 1-hour time point. Blots are representative of two independent experiments. (**B** and **C**) Violin plots of the $\log_2$ RPKM counts of H3K4me1 ChIP-seq for (B) C1 or (C) C2 enhancer locations. Line indicates the median of distribution. Data are from three WT mice and a single *Irf3*$^{-/-}$ mouse. Statistical evaluation used the Wilcoxon signed-rank test for paired data. (**D**) Scatterplots indicating the $\log_2$ RPKM H3K4me1 ChIP-seq counts from LPS-stimulated WT BMDMs (*x* axis) versus *Irf3*$^{-/-}$ (*y* axis) (top) or additionally supplemented with IFN-β (bottom). Colors indicate three different groups determined by FC cutoff thresholds of WT compared with *Irf3*$^{-/-}$ (WT/*Irf3*$^{-/-}$); C1.1 (purple) LFC > 0.5 in LPS and LFC > 0.5 in LPS + IFN-β; C1.2 (orange) LFC > 0.5 in LPS and LFC < 0.5 in LPS + IFN-β; C1.3 (gray) LFC < 0.5 in LPS. (**E**) Heatmap of the *z*-scored H3K4me1 ChIP-seq data from LPS-stimulated WT, *Ifnar*$^{-/-}$, and *Irf3*$^{-/-}$ BMDMs or additionally supplemented with IFN-β. Each column represents a single mouse. (**F**) Boxplots of the $\log_2$ RPKM counts of ATAC-seq (GSE234914) signal overlapping with C1.1, C1.2, or C1.3 enhancer locations in lipid A–stimulated WT or *Irf3*$^{-/-}$ BMDMs. Data are the average of two mice per condition. Statistical evaluation used the Wilcoxon rank-sum test for unpaired data. **P* < 0.05; ***P* < 0.001; ****P* < 0.0001. (**G**) Boxplots of the $\log_2$ RPKM counts of the IRF3 ChIP-seq (GSE67357) signal for lipid A–treated BMDMs overlapping with the C1.1, C1.2, or C1.3 enhancer locations. Data are the average of two mice per condition. Statistical evaluation used the Wilcoxon rank-sum test for unpaired data. **P* <0.05; ***P* < 0.001; ****P* < 0.0001. (**H**) Violin plots of the H3K4me1 LFC values for WT BMDMs stimulated with IFN-β (1 U/ml) or LPS (100 ng/ml). Line indicates the median of distribution. Data are from a single IFN-β–treated mouse or the average of three LPS-treated mice. (**I**) Heatmap of the *z*-scored H3K4me1 C&T data for 1548 locations induced (LFC > 2, FDR < 0.01) in human macrophages after 8 hours of stimulation with LPS (100 ng/ml), Pam3CSK (P3K; 100 ng/ml), or IFN-β (10 U/ml). Clusters generated by unsupervised *k*-means were subjected to de novo motif analysis. Each column represents a single technical replicate. Right: The top enriched sequence for each cluster. (**J**) Violin plots of the $\log_2$ RPKM counts of H3K4me1 C&T signals for cluster 1 locations. Data are an average of two replicates from the same human participant.

We next extended the study to human macrophages. We produced macrophages from peripheral blood mononuclear cells (PBMCs) with M-CSF and stimulated them with LPS and Pam3CSK (P3K) for 8 hours to identify NF-κB–driven and ISRE-containing de novo enhancers by CUT&Tag (C&T). *k*-means clustering revealed two major groups, with cluster 1 (1098 locations) being unresponsive to P3K and containing an ISRE as the most prominent motif and cluster 2 (450 locations) being responsive to P3K and containing an NF-κB motif as the most prominent motif (Fig. 2I). We then asked whether IFN-β could induce the de novo ISRE enhancers. We chose a concentration of IFN-β (10 U/ml) that was 10-fold greater than the saturating dose for expression of the canonical ISGF3 target gene *ISG15* (fig. S2). Even at this concentration, we found that IFN-β only partially induced de novo ISRE enhancers compared with LPS (Fig. 2, I and J). These results support the notion that ISGF3 is insufficient for complete formation of de novo ISRE enhancers in human

macrophages, consistent with our results from experiments with BMDMs (Fig. 2H).

### Formation of de novo IRF-associated enhancers requires the combinatorial activity of IRF1 and ISGF3

We hypothesized that the IRF family member IRF1 may act in concert with ISGF3 to produce ISRE de novo enhancers. IRF1 has primarily been studied in the context of type II IFN (IFN-γ) responses (*8*, *25*, *26*), but its expression was also induced by LPS-activated NF-κB (Fig. 3A). Furthermore, type I IFN–activated ISGF3 did not induce IRF1 expression, nor was ISGF3 activity reduced because of the lack of IRF1 activity (fig. S3A). These observations lead us to hypothesize that ISGF3 and IRF1 may collaborate to regulate de novo ISRE enhancer formation.

To test this hypothesis, we stimulated BMDMs of *Irf1*$^{-/-}$ mice with LPS and performed H3K4me1 ChIP-seq. Principal components analysis (PCA) of the previously identified set of 4800 LPS-induced enhancers showed that *Irf1*$^{-/-}$ BMDMs responded similarly to *Irf3*$^{-/-}$ and *Ifnar*$^{-/-}$ BMDMs (fig. S3B). To explore the relative contribution of these two factors, we used knockout data to compare with WT (WT/KO) and classified the LPS-induced enhancers into those that are ISGF3-dominant (group 1; LFC > 0.5, FDR < 0.05 in *Ifnar*$^{-/-}$), IRF1-dominant (group 2; LFC > 0.5, FDR < 0.05 in *Irf1*$^{-/-}$), IRF1- and ISGF3-dependent (group 3; LFC > 0.5, FDR < 0.05 in both *Irf1*$^{-/-}$ and *Ifnar*$^{-/-}$), or IRF1- and ISGF3-independent as a control group (group 4; FDR > 0.8) (Fig. 3, B to D). Whereas the WT H3K-4me1 median RPKM values averaged 2.3 to 2.4 $\log_2$ RPKM in each of the four groups, median RPKM values for *Ifnar*$^{-/-}$ cells were 1.4 and 1.5 in groups 1 and 3, respectively, and in *Irf1*$^{-/-}$ cells, they were 1.5 in both groups 2 and 3 ($P < 0.001$ for all comparisons) (Fig. 3C). In the control group, no effect was observed in either knockout cell (Fig. 3, C and D). The H3K4me1 counts in the basal state of all genotypes were highly correlated (>0.78 Spearman coefficient) for the four groups, suggesting that the poised enhancer landscape in naïve macrophages is not substantially affected by the absence of ISGF3 or IRF1 (fig. S3C). In addition, the IRF1- and ISGF3-dependent de novo enhancers were largely distinct from the earlier described IRF3-dependent de novo enhancers because only 9% of group 1, 12% of group 2, and 6% of group 3 enhancer regions overlapped with the enhancer locations of cluster C1.1 (fig. S3D), and no deficiency in IRF1 expression was observed in *Irf3*$^{-/-}$ BMDMs (fig. S3E).

Transcription factor motif enrichment analysis revealed only subtle differences in the connecting nucleotides between the half-sites of the ISRE: CT was most frequent in groups 1 and 3 versus GT in group 2. In addition, the 3′ end of the motif in group 1 was less well defined (fig. S3F). These differences may partially contribute to differential IRF binding (*19*, *27*). We examined available IRF1 and IRF9 ChIP-seq datasets of BMDMs stimulated with LPS or IFN-β, respectively (*23*, *28*), and determined the overlap of the IRF1 and IRF9 binding locations with the de novo enhancer locations (Fig. 3D). We found slightly higher rates of IRF1 binding at IRF1-dominant de novo enhancers (95%) than ISGF3-dominant de novo enhancers (76%) and slightly higher rates of IRF9 binding at ISGF3-dominant (75%) than IRF1-dominant de novo enhancers (67%). We observed similarly frequent binding of IRF1 and IRF9 in the IRF1- and ISGF3-dependent group 3 (>85%) and substantially less binding to locations within the IRF1- and ISGF3-independent control group (Fig. 3, D and E). The relative binding positions of IRF1 and IRF9 in relation to the H3K4me1 peaks followed a normal distribution centered at the midpoint of the H3K4me1 peak (fig. S3G), whereas the average peak width of IRF1 or IRF9 was slightly greater than 500 base pairs (bp), demonstrating a high level of specificity in the analyzed region (fig. S3H). Furthermore, IRF1 and IRF9 binding colocalized in >60% of group 1 and group 2 locations and >80% in group 3 enhancer locations (fig. S3I). In contrast, only 10% of group 4 locations had both IRF1 and IRF9 colocalized at the same locations. Together, these results suggest that, although subtle differences in ISRE motif variants and IRF1 and IRF9 binding rates could be identified between the groups, these appeared to be insufficient to explain the differential factor requirement in generating ISRE de novo enhancers.

### IRF1 and ISGF3 have sequential roles in the formation of ISRE de novo enhancers

To assess the mechanistic roles of IRF1 and ISGF3 in opening chromatin, we performed ATAC-seq on BMDMs stimulated with LPS (100 ng/ml) for 0 to 4 hours. We then found the overlap between ATAC-seq peaks and LPS-induced de novo enhancer regions. Using the same four groups determined earlier (Fig. 3), we observed similar overall trends of IRF1 versus ISGF3 dependency in chromatin opening (Fig. 4, A and B, and fig. S4, A to D). Furthermore, upon close examination of individual time points, we found that the deficiency in chromatin opening in *Ifnar*$^{-/-}$ BMDMs was not present until 2 hours, whereas *Irf1*$^{-/-}$ BMDMs diverged from WT cells within 1 hour of stimulation (Fig. 4, B and C, fig. S4, A to D). The temporal specificity in *Irf1* versus *Ifnar* requirement was more prominent for the highly IRF1-dependent groups (groups 2 and 3) than for the ISGF3-dominant group (group 1).

Next, we quantitatively compared the relationship between chromatin opening, as assessed by ATAC-seq, and the formation of de novo enhancers, as determined by ChIP-seq (Fig. 4D). As a reference point of comparison, we calculated the fraction of H3K4me1 signal loss in *Ifnar*$^{-/-}$ and *Irf1*$^{-/-}$ cells relative to WT cells at 8 hours for each location. We also calculated the fraction of ATAC-seq signal loss in *Ifnar*$^{-/-}$ and *Irf1*$^{-/-}$ cells relative to WT cells for each location at all three time points. We then used Spearman coefficients to determine whether loss of the ATAC-seq signal correlated with loss of the ChIP-seq signal. We found that, for both genotypes, at the 4-hour time point, losses of ATAC-seq signal correlated with losses of ChIP-seq signal, with $\rho > 0.4$ for all groups of locations (Fig. 4D). However, at early time points, in *Ifnar*$^{-/-}$ BMDMs, the ATAC-seq signal did not mirror the loss of the later ChIP-seq signal; this was especially evident at the 1-hour time point, where the correlation coefficient was near zero for all groups of locations (Fig. 4D). In contrast, the loss of ATAC-seq signal in *Irf1*$^{-/-}$ cells correlated with the loss of the subsequent ChIP-seq signal even at the 1-hour time point. These results suggest that IRF1 plays a critical role in the initial steps of opening chromatin, whereas ISGF3 is important in subsequent steps, with both factors being required for the formation of de novo enhancers.

If IRF1 plays a greater role in initiating chromatin opening at early time points, we hypothesized that, compared with IRF1-independent enhancers, IRF1-dependent enhancers may have less chromatin accessibility under basal conditions. To characterize the basal chromatin state, we investigated available BMDM datasets and found that group 2 and group 3, which are highly IRF1-dependent, showed lower ATAC-seq signals and less PU.1 and RNA Pol II binding than group 1, which contains locations that have a less strict requirement for IRF1 (Fig. 4, E to G). Together, these results suggest that IRF1

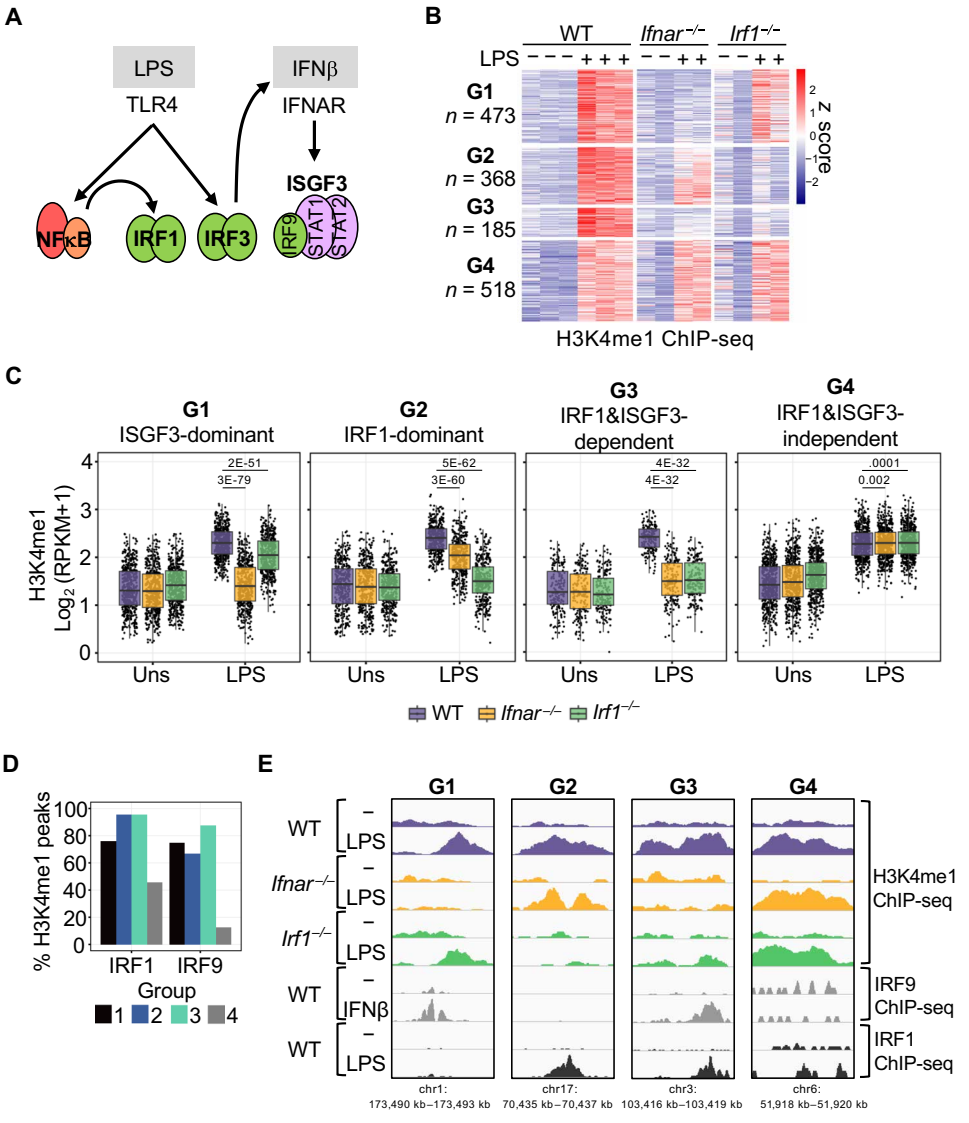


**Fig. 3. ISRE de novo enhancer formation requires both IRF1 and ISGF3.** (**A**) Schematic diagram of the LPS signaling network indicating control of IRF1 production by NF-κB. (**B**) Heatmap of the *z*-scored H3K4me1 ChIP-seq data after 8 hours of stimulation of WT, *Ifnar*$^{-/-}$, and *Irf1*$^{-/-}$ BMDMs with LPS. LPS-induced enhancers ($n$ = 4800) are grouped into those that are IFNAR-dependent (group 1; LFC > 0.5, FDR < 0.05; WT/*Ifnar*$^{-/-}$), IRF1-dependent (group 2; LFC > 0.5, FDR < 0.05; WT/*Irf1*$^{-/-}$), dependent on both factors (group 3; LFC > 0.5, FDR < 0.01; WT/*Ifnar*$^{-/-}$ and WT/*Irf1*$^{-/-}$), or independent of both factors (group 4; FDR > 0.8 in WT/*Ifnar*$^{-/-}$ and WT/*Irf1*$^{-/-}$). Each column represents a single mouse. (**C**) Boxplots of the $\log_2$ RPKM counts of H3K4me1 ChIP-seq for the groups determined in (B). Data are the average of two or three mice per condition. Statistical evaluation used the Wilcoxon signed-rank test for paired data. (**D**) Percentage of the H3K4me1 peaks overlapping with binding events of IRF1 (LPS stimulation) (GSE56123, data from a single mouse) or IRF9 (IFN-β stimulation) (GSE115435, data from two mice). (**E**) H3K4me1 genome browser tracks of representative de novo enhancer regions of G1, G2, G3, and G4.

plays a particularly critical role at locations where chromatin is tightly compacted and devoid of factors associated with enhancer priming and basal transcriptional activity.

## IRF1 functions in concert with ISGF3 or GAF to produce de novo enhancers

Having shown that IRF1 plays a critical role in chromatin remodeling downstream of LPS, we wondered whether IRF1 plays a similar role when induced by IFN-γ–activated GAF (Fig. 5A). Stimulation of macrophages with IFN-γ leads to broad chromatin remodeling (*8*, *14*, *29*), but it is not clear which SDTFs are responsible. Previous studies have suggested, by ChIP-seq analyses, that the ISGF3 components IRF9 and STAT2 aid IFN-γ–induced transcriptional activation (*23*) but not chromatin opening (*29*). To directly assess whether ISGF3 activity was induced in BMDMs upon stimulation with IFN-γ, we performed electrophoretic mobility shift assay (EMSA) with probes for GAF and ISGF3. Our data indicate that, whereas GAF was activated at the lowest concentration of IFN-γ (3 ng/ml), ISGF3 was not activated even by the greatest concentration (100 ng/ml) (fig. S5A). In addition, nuclear Western blots did not detect pSTAT2 upon stimulation by IFN-γ, whereas STAT1 and IRF1 were highly activated (fig. S5B).

To assess the role of IRF1 in IFN-γ–induced de novo enhancer formation, we performed H3K4me1 ChIP-seq on WT and *Irf1*$^{-/-}$ BMDMs stimulated with IFN-γ (100 ng/ml). We identified 2231 de novo enhancer regions by applying a cutoff of FDR < 0.01 and LFC > 0.5 on duplicate data from WT cells. Of these, 1820 IFN-γ–induced de novo enhancers were IRF1-dependent (FDR < 0.01, LFC > 0.5), whereas 411 appeared to be IRF1-independent (Fig. 5B). Motif enrichment analysis revealed that the top motif for IRF1-dependent enhancers was "IRF1," whereas that for IRF1-independent enhancers was "STAT1" (fig. S5C). Similar to the LPS-induced enhancers, we also observed that the basal chromatin state in WT BMDMs was less accessible in the IRF1-dependent group than in the IRF1-independent group (Figs. 4E and 5C). Furthermore, analysis of PU.1 and Pol II ChIP-seq data from BMDMs (*8*) revealed that, under

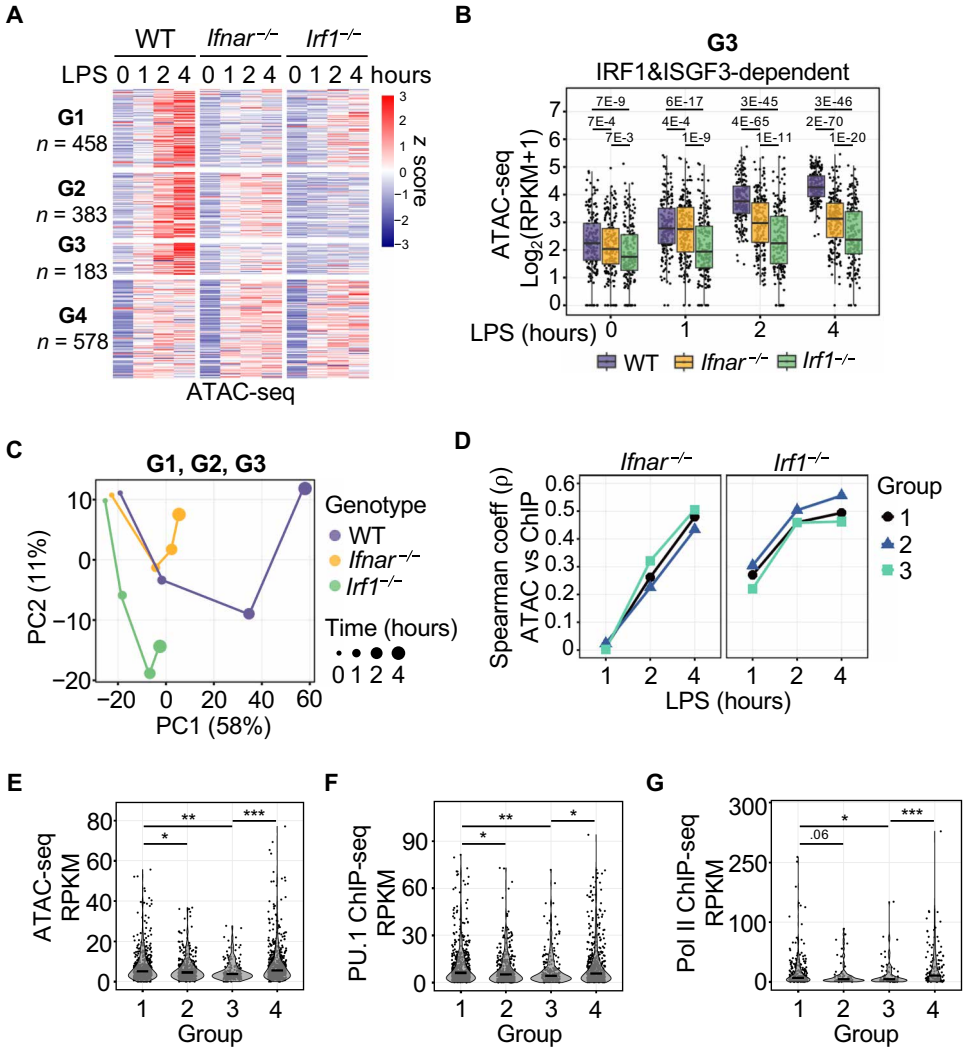


**Fig. 4. Early versus late temporal roles of IRF1 and ISGF3 in chromatin opening at ISRE de novo enhancer locations.** (**A**) Heatmap of the *z*-scored ATAC-seq signals from the peaks that overlap with de novo enhancer regions (Fig. 3B) after LPS stimulation for the indicated times. Each column represents a single mouse. (**B**) Boxplot of the $\log_2$ RPKM counts of ATAC-seq signal in group 3 (G3) locations, which are dependent on both ISGF3 and IRF1. No deficiency was observed in *Ifnar*$^{-/-}$ cells at the 1-hour time point. Data are from a single mouse per genotype. Statistical evaluation used the Wilcoxon signed-rank test for paired data. (**C**) PCA plots of the ATAC-seq signals from groups 1, 2, and 3 (G1 to G3), in cells of the indicated genotypes at the indicated times. (**D**) Spearman correlation analysis of the knockout H3K4me1 signal as a percentage of WT and the knockout ATAC-seq signal as a percentage of WT. Loss of the H4K4me1 signal in the knockout cells is generally mirrored by loss of ATAC-seq signal but not at the 1-hour time point for *Ifnar*$^{-/-}$ cells. (**E** to **G**) Violin plots of the RPKM counts of ATAC-seq, PU.1 ChIP-seq, or RNA Pol II ChIP-seq (GSE38377) in the basal state at regions overlapping with the G1 to G4 enhancer locations. Lines indicate the medians of the distributions. Each plot represents a single mouse. Statistical significance was determined by Wilcoxon rank-sum test for unpaired data. $*P < 0.05$; $**P < 0.001$; $***P < 0.0001$.

basal conditions, the genomic regions of IRF1-dependent de novo enhancers have reduced PU.1 and RNA Pol II binding compared with the IRF1-independent enhancers (Fig. 5, D and E). These results indicate that GAF remodels chromatin without IRF1 only at a minority of locations where the chromatin state is less compacted and where there is a greater extent of PU.1 and RNA Pol II binding; however, IRF1 is required for most IFN-γ–induced de novo enhancers, and these locations contain IRF-cognate ISREs.

We asked whether IRF1 cooperates with ISGF3 (when activated by LPS) or GAF (when activated by IFN-γ) at the same enhancer locations. Of the 1820 IFN-γ—induced, IRF1-dependent de novo enhancers and the 1026 LPS-induced, IRF1- or ISGF3-dependent de novo enhancers (groups 1 to 3; Fig. 3B), 567 locations (25%) passed the significance threshold as being induced by both LPS and IFN-γ with available datasets (Fig. 5F). However, it was apparent that, for the 459 LPS-dominant de novo enhancers (20%), stimulation with IFN-γ also led to a degree of activation, as did LPS for the 1258 IFN-γ–dominant de novo enhancers (55%). Focusing on the common LPS- and IFN-γ–induced locations, de novo motif analysis revealed an IRF1 binding consensus sequence (fig. S5D), which we had also identified in the ISGF3- and IRF1-dependent group 3 (fig. S3C).

We also explored the differences between LPS- and IFN-γ–induced de novo enhancers in human macrophages. H3K4me1 C&T on stimulated human macrophages revealed that there were 256 de novo enhancers induced by both LPS and IFN-γ, whereas 842 were predominantly induced by LPS and 391 predominantly by IFN-γ (fig. S5E). Whereas human macrophages derived from PBMCs appeared to produce fewer IFN-γ–induced enhancers than did mouse BMDMs, a marked overlap in type I and type II IFN–dependent locations was observed in both macrophage preparations. Motif enrichment analysis also confirmed that IRF1 motifs were present not only in LPS-induced de novo enhancers but also those in common and, to a lesser extent, those in the IFN-γ–dominant group, suggesting collaboration between IFN-γ–activated STAT1 (through GAF) and IRF1.

Using publicly available ChIP-seq data from mouse macrophages (*23*, *30*, *31*), we found that, of the 567 common de novo mouse enhancers, 354 showed STAT1 (GAF) binding in response to IFN-γ and 452 showed IRF9 (ISGF3) binding in response to

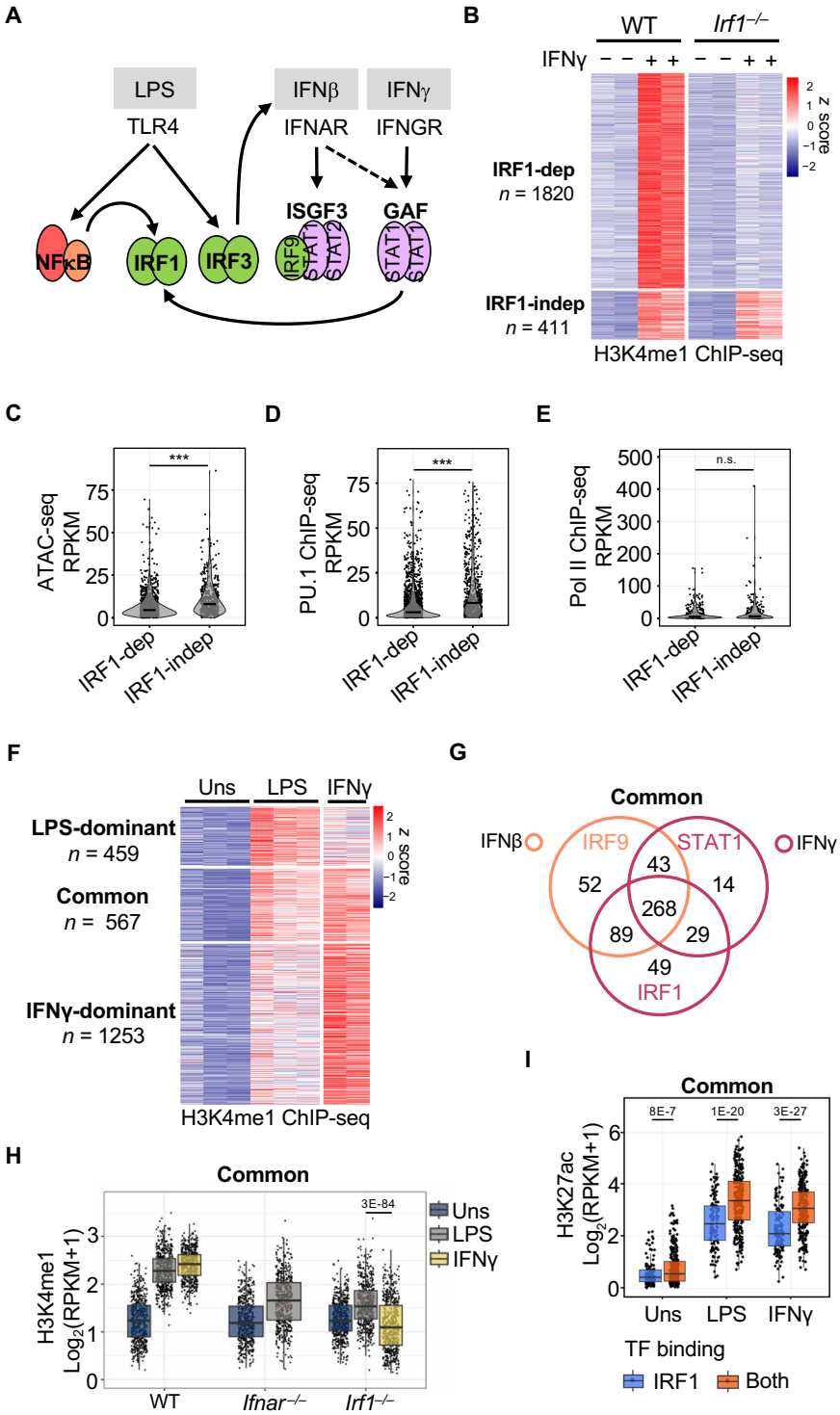


**Fig. 5. IRF1 cooperates with ISGF3 or GAF to stimulate IFN-γ–induced de novo enhancer formation.** (**A**) Schematic diagram of the LPS and IFN-γ signaling pathways. (**B**) Heatmap of the *z*-scored H3K4me1 ChIP-seq data showing 2231 regions induced after 8 hours of stimulation with IFN-γ (100 ng/ml) (LFC > 0.5, FDR < 0.01). IRF1-dependent and IRF1-independent clusters determined by FDR < 0.05, LFC > 0.5 were compared with WT. Each column represents a single mouse. (**C** to **E**) Violin plots of RPKM counts in the basal state of ATAC-seq (D), PU.1 ChIP-seq (E), and RNA Pol II ChIP-seq (GSE38377) in the IFN-γ–induced enhancer locations. Lines indicate the medians of the distributions. Each blot represents a single mouse. Statistical evaluation used the Wilcoxon rank-sum test for unpaired data. ***$P < 0.0001$. (**F**) Heatmap of the *z*-scored H3K4me1 ChIP-seq data showing 2279 regions induced by LPS or IFN-γ and dependent on *Ifnar* (for LPS) or *Irf1* (for LPS and IFN-γ). Regions were clustered as LPS-inducible (LFC > 0.5, FDR < 0.05) (LPS-dominant), IFN-γ–inducible (LFC > 0.5, FDR < 0.01) (IFN-γ–dominant), or inducible by both (common). Each column represents a single mouse. (**G**) Venn diagram of IRF1 (IFN-γ stimulation; GSE77886), STAT1 (IFN-γ stimulation; GSE115435 and GSE33913), and IRF9 (IFN-β stimulation; GSE115435) ChIP-seq peaks in the "common" de novo enhancer locations. Locations were derived from one or two mice. (**H**) Boxplot of the $\log_2$ RPKM counts of H3K4me1 ChIP-seq for the "common" locations in WT, *Ifnar*$^{-/-}$, and *Irf1*$^{-/-}$ BMDMs. Data are an average of two or three mice per condition. Statistical evaluation used the Wilcoxon signed-rank test for paired data. (**I**) Boxplot of the $\log_2$ RPKM counts of H3K27ac ChIP-seq under basal conditions or after 4 hours of stimulation with IFN-γ (100 ng/ml; GSE38377). Colors indicate locations with the indicated transcription factor (TF) binding. IRF1 = IRF1 binding, Both = IRF1 and STAT1 binding. Data are from a single mouse per condition. Statistical significance was determined by Wilcoxon rank-sum test for unpaired data.

LPS (Fig. 5G and fig. S5F). Their formation with either stimulus was highly dependent on IRF1 (Fig. 5H), indicating that IRF1 cooperates with either ISGF3 or GAF, depending on the stimulus, to induce de novo ISRE enhancer formation. Closer inspection of the *Irf1*$^{-/-}$ cell data revealed a stronger deficiency when IFN-γ was the stimulus (Fig. 5H). To further understand the cooperativity mechanism between GAF and IRF1 in these regions, we divided the common enhancer locations into those that had only IRF1 or both IRF1 and STAT1 ChIP-seq signals and compared their H3K27ac amounts (Fig. 5I). We observed greater H3K27ac abundance in response to either LPS or IFN-γ in the regions that had both IRF1 and STAT1 binding compared with those that had IRF1 only, suggesting that ISGF3 and GAF binding to these enhancer regions promoted the recruitment of enzymes that activate enhancers. Furthermore, among the LPS and IFN-γ common enhancer locations that had both IRF1 and STAT1 ChIP-seq signals, 57% of the IFN-γ–induced STAT1 peaks were associated with an ISRE motif and only 16% with a GAS motif (fig. S5G). In comparison, the STAT1 peaks in the IRF1-independent, IFN-γ–induced de novo enhancer locations were enriched by GAS motifs (43%) rather than ISRE motifs (26%). Together, these results suggest that IRF1 has the ability to recruit GAF to ISREs to form de novo enhancers in response to IFN-γ, for example, by binding directly to GAF, as previously suggested (*32*–*34*), in contrast with the sequential action of IRF1 and ISGF3 on ISREs in response to LPS.

### Genes near de novo enhancers show potentiated expression in response to subsequent immune challenge

Next, we examined whether IRF1-dependent enhancers altered macrophage transcriptional responses to a subsequent challenge. We stimulated WT BMDMs with IFN-γ for 8 hours, removed the stimulus, and let the cells rest for 64 hours. We then challenged the rested BMDMs with LPS (0.1 ng/ml) and collected samples at 0, 1.5, and 3 hours for RNA sequencing (RNA-seq) (Fig. 6A). To assess the effect of IFN-γ training on the LPS response, we first identified genes of interest as those whose expression was induced at LFC > 0.5 at least one time point upon LPS challenge under phosphate-buffered saline (PBS) or IFN-γ–trained conditions. For the resulting 1337 genes, we calculated the effect of IFN-γ at the 3-hour time point when compared with the PBS control and divided these fold changes into 10 bins (fig. S6A). In general, bins 1 to 5 were enriched for genes with Gene Ontology (GO) terms related to metabolic and growth processes, whereas genes in bin 6 and higher were enriched for "response to external biotic stimulus" or "response to other organism" (fig. S6B). Bin 10 had the highest enrichment of GO terms, and "response to interferon-beta" was statistically significant only in this group. These results suggest that IFN-γ tolerizes the induction of genes encoding factors involved in metabolic pathways, whereas it potentiates the expression of genes encoding factors in inflammatory pathways and responses to innate immune challenges.

Next, we assessed the expression of genes closest to the previously identified 1820 IRF-dependent, IFN-γ–induced de novo enhancers (Fig. 5B) and identified 791 unique genes (Fig. 6B). We clustered them on the basis of their expression response to LPS by the *k*-means algorithm into three groups (I1 to I3) (Fig. 6B). We found that cluster 1 (I1) genes were not induced by LPS, and there was very little enrichment of GO terms (Fig. 6C). Cluster 2 (I2) genes were diminished by IFN-γ training and were enriched for GO terms related to metabolic pathways. Cluster 3 (I3) genes showed potentiated LPS responsiveness after IFN-γ training. The top GO terms for cluster 3 were "response to external biotic stimulus," "innate immune response," and "cellular response to type II IFN" (Fig. 6C).

We then tested the IRF1 dependency of these genes. We found that, for cluster 3 genes, the potentiation effect by IFN-γ was abrogated in *Irf1*$^{-/-}$ BMDMs. When looking at the LPS-inducible genes of cluster 3 (LFC > 0.5), the potentiation effect of IFN-γ was reduced in *Irf1*$^{-/-}$ cells when viewed in a pairwise comparison of fold changes ($P < 0.001$; Fig. 6D). Genes in cluster 3 included *Ifit3* and *Mx1*, which encode antiviral effectors (Fig. 6E). Together, these results suggest that IRF1-dependent enhancers are associated with the potentiation of nearby genes that are also IRF1-dependent.

We next asked whether LPS-induced, IRF-dependent enhancer formation correlated with the potentiation of gene expression responses. Although it is well established that LPS treatment leads to an overall state of tolerance, whereby cells respond to a second stimulation with lower inflammatory gene expression (*4*), genes related to tissue repair and antimicrobial effectors may be expressed to a greater extent (*35*). We trained macrophages with LPS (100 ng/ml) for 8 hours and then challenged them with LPS (0.1 ng/ml) after 72 hours. We found 1192 genes that were within 100 kb of LPS-induced IRF-dependent enhancers. We filtered for those genes that were inducible at at least one time point of secondary LPS exposure either in PBS or LPS-trained macrophages (LFC > 0.5) and found 225 genes that clustered in two distinct clusters (L1 and L2) by the *k*-means algorithm (Fig. 6F). Cluster 1 (L1) was characterized by tolerized genes that were enriched for GO terms such as "regulation of gene expression" and "regulation of cytokine production." Furthermore, cluster 2 (L2) was characterized by potentiated genes that were strongly enriched for the GO terms "response to external biotic stimulus," "response to other organism," and "response to IFN-β" (Fig. 6G). In addition, we observed a decrease in the potentiation of L2 genes upon LPS training in both *Ifnar*$^{-/-}$ and *Irf1*$^{-/-}$ macrophages (fig. S6C). These results suggest that IRF-regulated enhancers potentiate the expression of a subset of LPS-responsive genes in a manner that is dependent on IRF1 and ISGF3.

### A pathway map for ISRE de novo enhancers

Together, these findings identify the regulatory logics of IRF family members and their collaborative relationships with STAT transcription factors that are responsible for the formation of de novo enhancers induced by LPS and type II IFN (IFN-γ). Our data support a stepwise model of enhancer formation (Fig. 7A), which has four distinguishable steps: (i) Compacted chromatin that has low accessibility as determined by ATAC-seq analysis must first be opened before (ii) nucleosomes are fully displaced. Nucleosome displacement is a prerequisite for (iii) recruiting RNA polymerase and histone-modifying enzymes to activate the de novo enhancer (H3K27Ac marks) before (iv) the enhancer assumes a poised state with H3K4me1 marks (but no H3K27ac marks) within a few hours but that is long-lasting for the week-long duration of the experiment. We found that de novo enhancers may be generated from either highly compacted, low-accessibility latent enhancer regions or moderate-accessibility latent enhancer regions. The former show a strict IRF1 requirement to provide the initial chromatin opening that may then be extended by the collaborating factors ISGF3 or GAF. The latter show a less strict requirement for IRF1, with GAF or ISGF3 being able to extend chromatin accessibility and induce enhancer marks.

This model informs a pathway map of distinct classes of de novo enhancers (Fig. 7B). De novo enhancers are distinguished by their association with the DNA binding motifs of SDTFs, their stimulus-specific inducibility, their genetic requirement for SDTF family members, and their chromatin compactness versus accessibility in the basal, naïve state. For example, of the 4800 LPS-induced de novo enhancers in our experiments, 2688 are induced by NF-κB, 220 by IRF3, and 1892 by a combination of IRF1 and ISGF3, which function sequentially. The degree of IRF1 requirement appears to be determined by their chromatin accessibility in the basal state. Similarly, of the 2200 IFN-γ–induced de novo enhancers in our experiments, 1820 show a strict IRF1 requirement and low accessibility, induced by the combinatorial IRF1-GAF action through ISRE sites, whereas 411 appear to be induced solely by GAF from a moderate accessibility state through GAS sites. Low-accessibility ISRE de novo enhancers therefore require the combined action of IRF1 with either ISGF3 (in response to LPS) or GAF (in response to IFN-γ). In contrast, NF-κB–induced de novo enhancers require a nonoscillatory activity that emanates from MyD88-mediated stimuli (*14*). The biological implication of both is that, during an innate immune response, de novo enhancers are formed only in cells directly exposed to pathogen and not in bystander macrophages that are exposed to paracrine cytokines, such as TNF (*14*) or type I IFN, which are secreted by the primary responders.

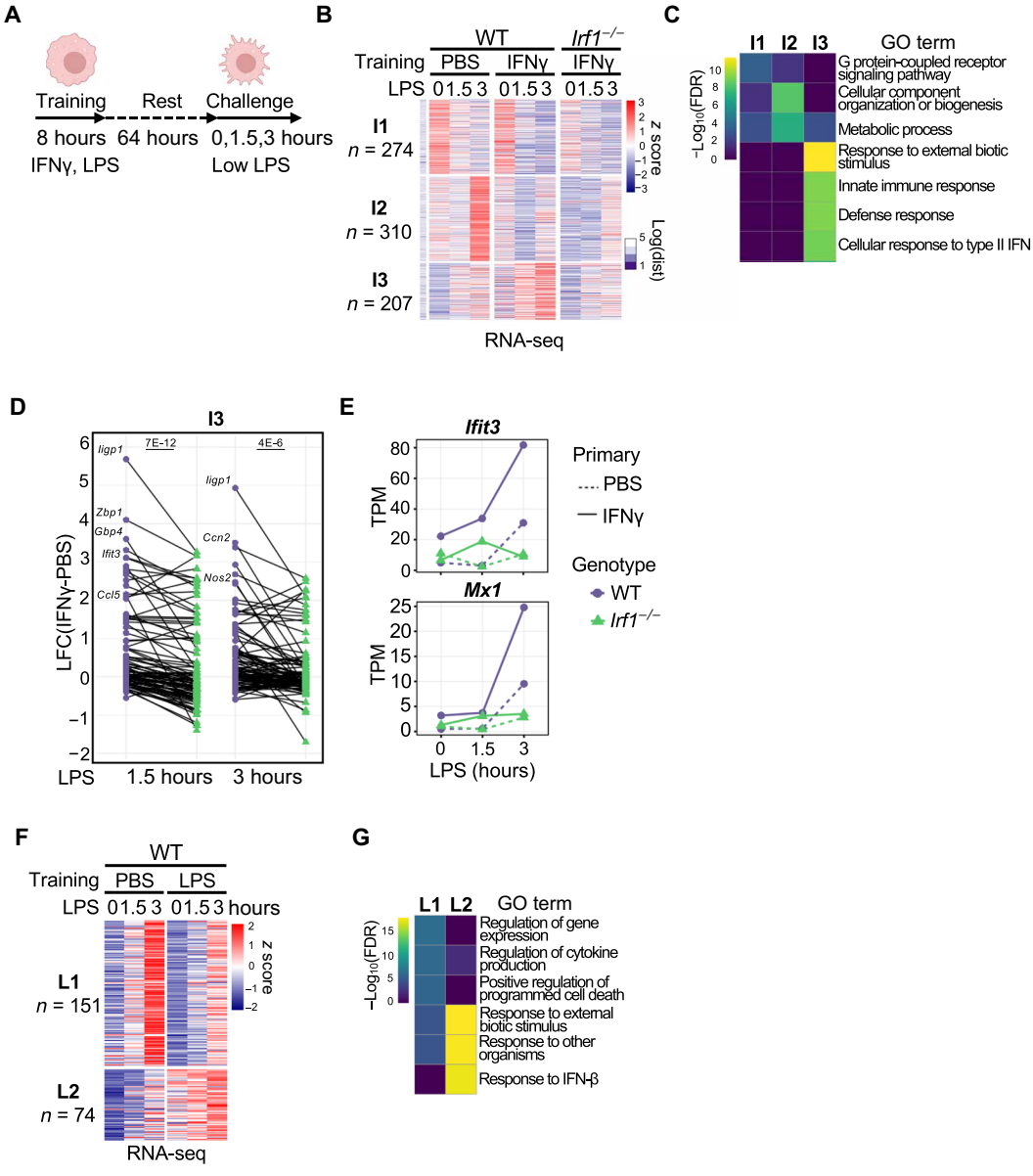


**Fig. 6. De novo enhancers direct gene expression responses to a subsequent immune challenge.** (**A**) Experimental scheme for the induction of innate immune memory. (**B**) Heatmap of the *z*-scored RNA-seq data from WT and *Irf1*$^{-/-}$ BMDMs trained with IFN-γ and rechallenged with LPS, showing the nearest expressed genes to IRF1-dependent, IFN-γ de novo enhancers (Fig. 4B). *k*-means clustering revealed three clusters (I1 to I3), where cluster 3 (I3) is potentiated by IFN-γ training. Each column represents a single mouse. (**C**) Heatmap showing the most highly enriched GO terms for the three clusters (I1 to I3) in (B). (**D**) Paired dot plot showing the training effect ($log_2$FC) of IFN-γ on LPS-inducible cluster 3 genes (LFC > 0.5), comparing the WT (purple) and *Irf1*$^{-/-}$ (green) genotypes. Statistical evaluation used the Wilcoxon signed-rank test for paired data. (**E**) Line plots of representative cluster 3 (I3) genes showing the effect of IFN-γ training in WT and *Irf1*$^{-/-}$ BMDMs. Data are from a single mouse per condition. (**F**) Heatmap of the *z*-scored RNA-seq data from BMDMs trained with LPS (100 ng/ml) and rechallenged with LPS (0.1 ng/ml), showing genes within 100 kb of enhancers that are LPS-inducible and IRF1- or IFNAR-dependent (Fig. 2B; groups 1, 2, and 3). *k*-means clustering revealed two clusters, where cluster 2 is potentiated by LPS training. Each column represents a single mouse. (**G**) Heatmap showing the most highly enriched GO terms for the two clusters in (F).

## DISCUSSION

After pathogen infection, it is critical that the host mounts an appropriate immune response quickly. Innate immune memory in macrophages is a mechanism by which a response to future infections may be fine-tuned and rendered more rapid or efficacious. The fitness rationale may be that conditions that involve pathogen exposure and immune activity may be predictive of further pathogen exposure and the need to mount immune responses. Our results provide evidence for IRF1 as a key epigenomic reprogramming factor in macrophages but one that must cooperate with STATs to establish de novo enhancers. During the innate immune response to PAMPs, the type I IFN–induced transcription factor ISGF3, which consists of STAT1, STAT2, and IRF9, extends IRF1-opened latent enhancer regions, whereas in the context of type II IFN (IFN-γ), typically provided by activated T cells, the transcription factor GAF (a STAT1

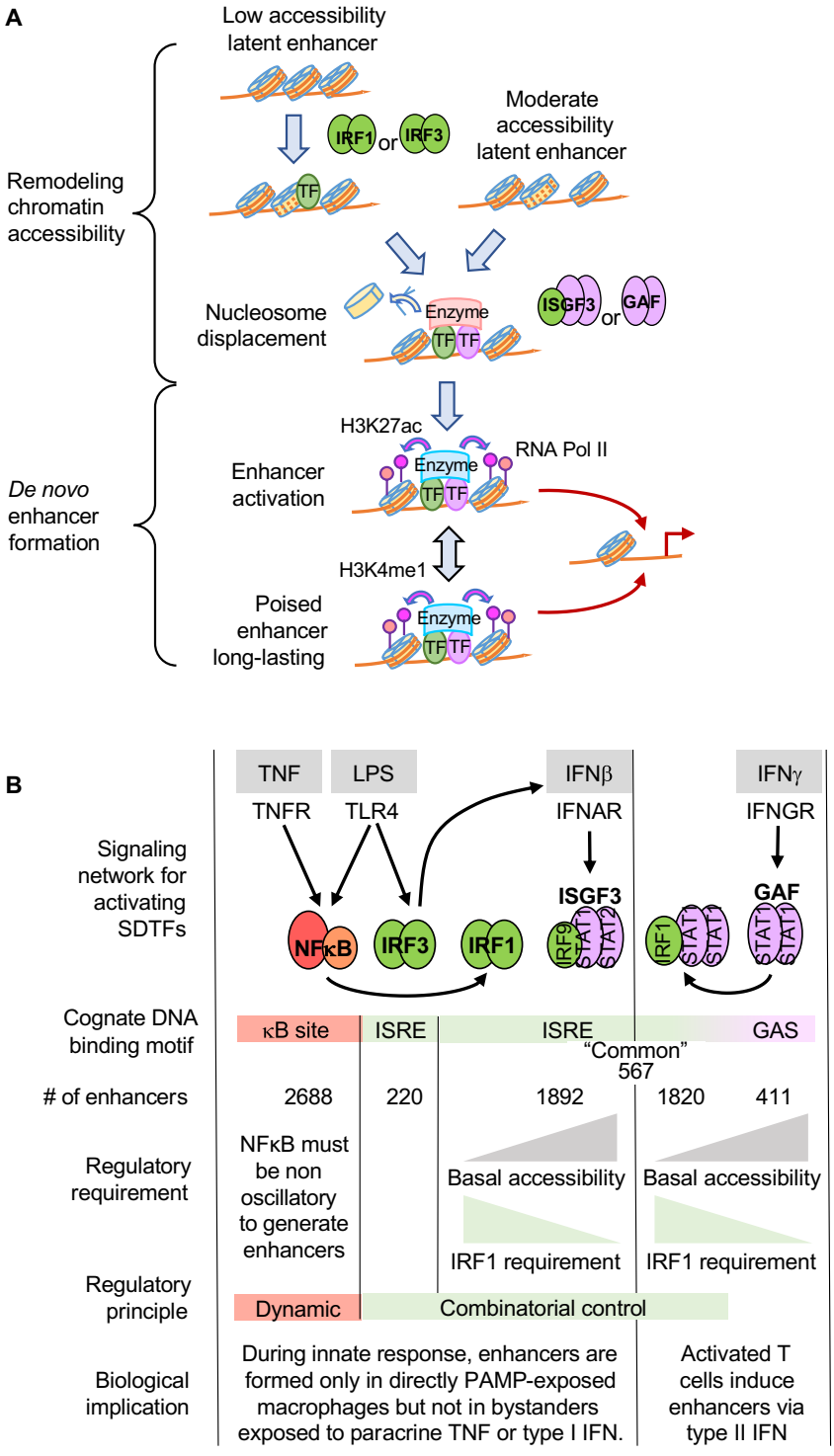


**Fig. 7. Pathway map for the formation of innate immune de novo enhancers.** (**A**) Model schematic of the de novo enhancer formation pathway. The first steps involve chromatin remodeling to increase accessibility. Locations with low accessibility in naïve macrophages require IRF3 or IRF1. Once moderate accessibility is achieved, ISGF3 or GAF may extend it. The subsequent steps involve transient enhancer activation by ISGF3 or GAF, as evidenced by PU.1 and RNA Pol II recruitment; H3K27Ac modification; and then the establishment of a durable poised state whose hallmark is H3K4me1 marks. (**B**) Pathway summary of innate immune de novo enhancers. From top to bottom, transcription factors induced by TNF, LPS, IFN-β, or IFN-γ function through their indicated cognate DNA binding motifs to induce the formation of the indicated number of de novo enhancers determined in this study, subject to the indicated regulatory requirements. Note that many of the LPS- and IFN-γ–induced locations overlap. Whereas the stimulus specificity of NF-κB–regulated enhancers is achieved by dynamic control principles, the stimulus specificity of IRF-regulated enhancers is achieved by combinatorial control principles. However, the biological implication is the same: Only directly pathogen-exposed cells, not bystanders, induce innate immune de novo enhancers on a large scale.

homodimer) may combine with IRF1 to induce overlapping sets of de novo enhancers.

Our studies involved newly generated epigenomic profiling datasets from genetic knockouts defective in specific IRFs to classify ISRE de novo enhancers and then leveraged datasets from a number of leading laboratories in the field to characterize these enhancers further. The results paint a picture that is consistent given the numerous subtle differences in experimental protocols among different laboratories over an almost 10-year period and supports the robustness and reliability of our conclusions in mouse macrophages. Our results with human macrophages suggest that key conclusions are consistent; however, further molecular characterization in human cells may be warranted.

We found that latent enhancer regions are first opened to increase accessibility, as revealed by ATAC-seq, before recruiting the pioneer factor PU.1 and RNA Pol II, acquiring histone modifications of de novo enhancers, and being transiently activated (H3K27Ac). After a few hours, they lose the activation mark but remain in a long-lasting poised state characterized by the H3K4me1 modification. The innate immune gene expression response of macrophages by LPS is initiated by IRF3 and amplified by ISGF3. Previous investigations determined that IRF3, although required for IFN-β production, appears to make few direct contributions to the large innate immune gene expression program (*19*). One outlier is the gene *Ccl5*, which requires a nucleosome remodeling event for full activation (*22*). Our studies extend this observation by identifying more than 200 genomic locations at which IRF3 is required for nucleosome remodeling and thus de novo enhancer formation. However, although this is a large number, it is dwarfed by the more than 1000 locations that show de novo enhancer formation in a manner that involves ISGF3 but not IRF3. Instead, ISGF3 cooperates with NF-κB–induced IRF1 to establish de novo enhancers. What sequence or topological chromatin features render a location IRF3-regulated versus IRF1-ISGF3–regulated remains unclear. Our studies

were unable to identify distinct ISRE sequence variants or other chromatin hallmarks. We recognize that IRF7 might be compensating for the loss of IRF3 in *Irf3*$^{-/-}$ BMDMs, expanding the number of de novo enhancers that are formed by IRF3 and IRF7; however, given the requirement for IRF1, we expect that the combined action of IRF3 and IRF7 stimulates enhancer formation only at a minority of locations.

The cooperation between IRF1 and ISGF3 appears to be through sequential actions that are both required for the formation of de novo enhancers. Although ISGF3 is activated within 1 hour of LPS stimulation, it is not functionally required until 2 hours, whereas IRF1 deficiency results in defects in chromatin opening by 1 hour. The engagement of two stimulus-induced factors in a sequence of required steps results in a logical AND gate of combinatorial synergy, even if the factors do not interact or bind each other. Other examples of this logic include the stimulus-induced expression of many inflammatory cytokine genes that depend on NF-κB–dependent transcriptional synthesis of mRNA and p38-dependent extension of the mRNA half-life, thereby forming a logical AND gate despite acting at different, albeit sequential, biochemical steps and in different subcellular compartments (*36*).

In the context of IFN-γ signaling, where ISGF3 inducibility was not detected, we demonstrated the cooperative action of IRF1 with GAF in forming de novo enhancers. Previous studies have shown the formation of a complex between STAT1 and IRF1 (*32*–*34*) or direct contact between STAT1 and IRF1 through chromatin looping (*25*, *37*). We showed that the IRF1 requirement was more stringent in macrophages stimulated with IFN-γ than in those stimulated with LPS while showing induced STAT1 binding. In addition, we found that STAT1 and GAF were colocalized with IRF1 binding locations that are enriched in ISRE sites. These observations are consistent with a model of direct cooperation between IRF1 and GAF cooperation, as opposed to the sequential model of action of the IRF1-ISGF3 pair. Furthermore, we observed greater amounts of H3K27ac in enhancer regions that were bound by ISGF3 (in response to LPS) or GAF (in response to IFN-γ). Other studies have previously reported that, in the IFN-γ response, STAT1 binds to sites that are already occupied by IRF1, inducing epigenomic activation of H3K27ac (*34*). These results suggest that, whereas IRF1 is required to initiate chromatin opening, GAF is needed to recruit enzymes that deposit epigenetic marks.

The biochemical characteristics of IRF1 and ISGF3-GAF may determine which biochemical steps each catalyzes. We note, for example, that the smaller size of IRF1 (37 kDa; potentially functioning as a monomer) (*38*) may enable it to function as a pioneer factor in opening nucleosomal DNA at genomic regions where chromatin is tightly compacted, whereas the larger ISGF3 complex may stabilize and extend partially accessible DNA locations. The prominent STAT1 activation domain may enable particularly efficient recruitment of histone-modifying enzymes and RNA polymerase to establish and transiently activate the de novo enhancer (*34*, *39*, *40*).

Whereas our analysis of IFN-γ–induced de novo enhancers identified and focused on IRF1-independent enhancers that contain GAS motifs and IRF1-dependent enhancers that contain ISREs and largely overlap with LPS-induced enhancers, there may also be de novo enhancers that require both IRF1 and GAF that function through their respective ISRE and GAS sites. The combinatorial versatility is expanded by the fact that both ISRE and GAS elements are composed of GAAA half-sites, arranged in the former as direct repeats and in the latter as palindromes, which means that three half-sites may be sufficient for both IRF3 and GAF to function independently or sequentially.

Because IRF1 production must be stimulus-induced, either through PAMP-stimulated NF-κB activity or IFN-γ–stimulated GAF activity, the combinatorial requirement of IRF1 and a partner SDTF ensures that de novo enhancers are not formed in all cells that are exposed to paracrine type I IFN. Type I IFN–exposed cells are warned of a nearby infection and induce antiviral and other innate immune genes but will not undergo substantial epigenomic reprogramming. In contrast, exposure to pathogen (which activates NF-κB through pattern recognition receptors) or CD4$^{+}$ T helper 1 cells (which secrete IFN-γ) will reprogram the epigenome of macrophages. Such specificity through a combinatorial control mechanism mirrors the specificity of NF-κB–regulated enhancers, which are also only induced by PAMPs (*14*) or when conditioning with IFN-γ potentiates NF-κB activation (*41*). Thus, two fundamental gene regulatory mechanisms that govern stimulus-specific gene expression, combinatorial and dynamic control (*42*, *43*), also govern the stimulus specificity of innate immune de novo enhancer formation through the IRF-STAT and NF-κB signaling pathways, respectively.

## MATERIALS AND METHODS

### Animals, cell culture, and stimuli

WT and specific gene-deficient C57BL/6 mice were housed and handled according to guidelines established by the UCLA Animal Research Committee under protocols ARC-2014-110 and ARC-2014-126. Bone marrow was isolated, and cells were grown as previously described (*44*). Cells were stimulated on day 7 with LPS (100 ng/ml; L6529-1MG, Sigma-Aldrich), IFN-β (1 U/ml; 12401-1, PBL Assay Science), or IFN-γ (100 ng/ml; 485-MI, R&D Systems) for the times indicated in the figure legends. Human blood from deidentified human participants was obtained from the UCLA CFAR Centralized Laboratory Support Core, according to IRB 11-000443. PBMCs were isolated by Ficoll (Cytiva) gradient centrifugation. Monocytes were purified from PBMCs with human CD14 microbeads (130-050-201, Miltenyi) according to the manufacturer's protocol. Monocytes were plated on six-well plates at a density of $1.2 \times 10^6$ cells per well and cultured for 7 days in 3 ml of RPMI supplemented with 10% fetal bovine serum (Omega), penicillin-streptomycin, and human M-CSF (25 ng/ml; 300-25, PeproTech). M-CSF was refreshed on day 5 of culture by restoring the concentration to 25 ng/ml (assuming that all M-CSF was depleted). On day 7, mature macrophages were stimulated with LPS (100 ng/ml; L6529-1MG, Sigma-Aldrich), human IFN-γ (100 ng/ml; 100-2, PeproTech), human IFN-β (10 U/ml; 11415, PBL Assay Science), or Pam3CSK4 (100 ng/ml; tlrl-pms, InvivoGen) for 8 hours.

### Biochemical analysis

Nuclear extracts were collected as previously described (*44*). For Western blotting analysis, the following antibodies were used: rabbit anti-IRF1 (Santa Cruz Biotechnology, sc640), mouse anti-pSTAT1 (Santa Cruz Biotechnology, sc136229), rabbit anti-pSTAT2 (Sigma-Aldrich, 07-224), mouse anti-IRF9 (MilliporeSigma, MABS1920), and rabbit anti-p84 (Abcam, ab131268), followed by mouse anti-rabbit IgG-HRP (Cell Signaling Technology, 7074) or anti-mouse IgG-HRP (Cell Signaling Technology, 7076). EMSA was performed as previously described (*44*, *45*). For the ISRE consensus sequence, we used 5′-GATCCTCGGGAAAGGGAAACCTAAACTGAAGCC-3′ and 5′- GGCTTCAGTTTAGGTTTCCCTTTCCCGAGGATC-3′;

for the GAS consensus sequence, we used 5′-TACAACAGCCTG-ATTTCCCCGAAATGACGC-3′ and 5′- GCGTCATTTCGGGGA-AATCAGGCTGTTGTA-3′; and for the NFY consensus sequence, we used 5′-GATTTTTTCCTGATTGGTTAAA-3′ and 5′- ACTTTTA-ACCAATCAGGAAAAA-3′ as a loading control.

### ChIP-seq analysis

Chromatin immunoprecipitation was performed as previously described (*14*). ChIP-seq libraries were prepared with the NEBNext Ultra II DNA Library Prep Kit (New England Biolabs, E7645). Libraries were single-end sequenced with a length of 50 bp on an Illumina HiSeq 3000. Reads were processed and aligned to the mouse genome (mm10) as previously described (*14*). Model-based analysis of ChIP-seq (MACS2/MACS3) (*46*) was used to call peaks at 1% FDR. We generated two reference peak files by merging the peaks under the LPS or IFN-γ (+unstimulated control) conditions in WT cells. We used these genomic locations to count the fragments in the WT and knockout samples for each stimulus condition with deeptools multiBamSummary (*47*). We used edgeR (*48*) to determine the significantly induced regions by applying a cutoff of FDR < 0.05 and LFC > 0.5 (LPS) or FDR < 0.01 and LFC > 0.5 (IFN-γ) compared with the unstimulated condition in WT cells. For the IRF1- or IFNAR-dependent groups (Fig. 2), significant peaks were identified by applying a cutoff of FDR < 0.05 and LFC > 0.5 in WT versus *Irf1*$^{-/-}$ or *Ifnar*$^{-/-}$ conditions, and the control group was identified by an FDR > 0.8 in WT versus *Irf1*$^{-/-}$ and *Ifnar*$^{-/-}$ in the LPS-inducible peaks. IRF1-dependent or IRF1-independent groups (Fig. 4) were defined by applying a cutoff of FDR < 0.05 and LFC > 0.5 comparing duplicates of IFN-γ–stimulated WT and *Irf1*$^{-/-}$ samples. Analysis of de novo transcription factor motif enrichment was performed with the findMotifsGenome function in the HOMER suite (*21*), using all detected peaks in the WT as background. Data were visualized with ggplot2 or the pheatmap packages in R. The following ChIP-seq datasets from BMDMs were obtained from Gene Expression Omnibus (GEO): H3K27ac (LPS or IFN-γ stimulation; GSE38377), PU.1 (LPS or IFN-γ stimulation; GSE38377), RNA Pol II (LPS stimulation; GSE38377), IRF3 (lipid A stimulation; GSE99895), IRF9 (IFN-β stimulation; GSE77886), IRF1 (LPS stimulation; GSE56123), IRF1 (IFN-γ stimulation; GSE77886), and STAT1 (IFN-γ stimulation; GSE115435 and GSE33913) (*8*, *22*, *23*, *28*, *30*, *31*). Raw datasets were aligned against mm10 as previously described (*14*). MACS (MACS3) (*46*) was used to call peaks at 1% FDR. A merged file was obtained for each transcription factor, and overlaps with the stimulus-specific H3K4me1 peaks were determined with the intersect function of the Bedtools package (*49*).

### C&T analysis

Mature stimulated and unstimulated macrophages were lifted from plates with 0.5 mM EDTA in PBS and gentle scraping. Nuclear isolation and tagmentation were performed with the CUTANA CUT&Tag Kit (Epicypher) according to the manufacturer's protocol and as previously described (*50*) with the anti-H3K4me1 antibody (Abcam, ab8895). Libraries were sequenced with paired-end, 50-bp reads on an Illumina NovaSeq X Plus. Reads were processed as described for ChiP-seq with the exception that the reads were aligned to the human hg38 genome. C&T peaks were called with MACS3 version 3.0.0b1 with standard options except -f BAMPE and -q 0.01. Differential peaks were identified as described for ChIP-seq with the exception that an LFC of 2.0 and FDR of 0.01 were used for all conditions. Motif analysis was performed as described earlier with the HOMER suite using the entire genome for background.

### ATAC-seq analysis

ATAC was performed as previously described (*14*). Libraries were prepared with the Nextera DNA Library Preparation Kit (Illumina, FC-121) and single-end sequenced (50 bp) on an Illumina HiSeq 3000. Sequenced reads were processed and aligned to the mouse genome (mm10) as previously described (*14*). MACS (MACS2) (*46*) was used to call peaks at 1% FDR. The peaks for all the ATAC-seq samples were used to generate a single reference peak file, and the number of reads that fell into each peak was counted with deeptools multiBamSummary (*47*). The overlap between the ATAC-seq and ChIP-seq peaks was determined with the intersect function of the Bedtools package (*49*). Reads were normalized by RPKM. Data were visualized with ggplot2 or the pheatmap packages in R. The lipid A–treated WT and *Irf3*$^{-/-}$ BMDM datasets were obtained from GEO (GSE234914).

### RNA-seq analysis

BMDMs were lysed with TRIzol reagent (Life Technologies), and total RNA was purified with the Direct-zol RNA MiniPrep kit (Zymo Research). RNA samples were submitted to BGI Genomics for selection of polyadenylated RNA and paired-end library preparation. Samples were sequenced on the DNBSEQ Technology platform (100 bp). Raw data were filtered for adaptor sequences or low-quality sequences with SOAPnuke. Reads were aligned to the mm10 genome with STAR (*51*). Aligned reads were processed as previously described (*14*). Data were normalized by transcript per million (TPM). Genes with TPM > 5 under at least two conditions were selected. The LPS-inducible genes were determined by applying a cutoff of LFC > 0.5 in at least one time point in the PBS, IFN-γ, or LPS conditions. The closest genes to the IFN-γ enhancers and the LPS-inducible genes within ±100 kb were based on linear proximity to the TSSs. Data were visualized with ggplot2 or the pheatmap packages in R.

## Supplementary Materials

**The PDF file includes:**
Figs. S1 to S6

**Other Supplementary Material for this manuscript includes the following:**
MDAR Reproducibility Checklist

## REFERENCES AND NOTES


1. K. M. Sheu, A. Hoffmann, Functional hallmarks of healthy macrophage responses: Their regulatory basis and disease relevance. *Annu. Rev. Immunol.* **40**, 295–321 (2022).
2. M. G. Netea, J. Domínguez-Andrés, L. B. Barreiro, T. Chavakis, M. Divangahi, E. Fuchs, L. A. B. Joosten, J. W. M. van der Meer, M. M. Mhlanga, W. J. M. Mulder, N. P. Riksen, A. Schlitzer, J. L. Schultze, C. Stabell Benn, J. C. Sun, R. J. Xavier, E. Latz, Defining trained immunity and its role in health and disease. *Nat. Rev. Immunol.* **20**, 375–388 (2020).
3. P. J. Murray, J. E. Allen, S. K. Biswas, E. A. Fisher, D. W. Gilroy, S. Goerdt, S. Gordon, J. A. Hamilton, L. B. Ivashkiv, T. Lawrence, M. Locati, A. Mantovani, F. O. Martinez, J.-L. Mege, D. M. Mosser, G. Natoli, J. P. Saeij, J. L. Schultze, K. A. Shirey, A. Sica, J. Suttles, I. Udalova, J. A. van Ginderachter, S. N. Vogel, T. A. Wynn, Macrophage activation and polarization: Nomenclature and experimental guidelines. *Immunity* **41**, 14–20 (2014).
4. S. K. Biswas, E. Lopez-Collazo, Endotoxin tolerance: New mechanisms, molecules and clinical significance. *Trends Immunol.* **30**, 475–487 (2009).
5. M. A. Dobrovolskaia, S. N. Vogel, Toll receptors, CD14, and macrophage activation and deactivation by LPS. *Microbes Infect.* **4**, 903–914 (2002).

6. S.-C. Cheng, J. Quintin, R. A. Cramer, K. M. Shepardson, S. Saeed, V. Kumar, E. J. Giamarellos-Bourboulis, J. H. A. Martens, N. A. Rao, A. Aghajanirefah, G. R. Manjeri, Y. Li, D. C. Ifrim, R. J. W. Arts, B. M. J. W. van der Veer, P. M. T. Deen, C. Logie, L. A. O'Neill, P. Willems, F. L. van de Veerdonk, J. W. M. van der Meer, A. Ng, L. A. B. Joosten, C. Wijmenga, H. G. Stunnenberg, R. J. Xavier, M. G. Netea, mTOR- and HIF-1α-mediated aerobic glycolysis as metabolic basis for trained immunity. *Science* **345**, 1250684 (2014).
7. S. Saeed, J. Quintin, H. H. D. Kerstens, N. A. Rao, A. Aghajanirefah, F. Matarese, S.-C. Cheng, J. Ratter, K. Berentsen, M. A. van der Ent, N. Sharifi, E. M. Janssen-Megens, M. Ter Huurne, A. Mandoli, T. van Schaik, A. Ng, F. Burden, K. Downes, M. Frontini, V. Kumar, E. J. Giamarellos-Bourboulis, W. H. Ouwehand, J. W. M. van der Meer, L. A. B. Joosten, C. Wijmenga, J. H. A. Martens, R. J. Xavier, C. Logie, M. G. Netea, H. G. Stunnenberg, Epigenetic programming of monocyte-to-macrophage differentiation and trained innate immunity. *Science* **345**, 1251086 (2014).
8. R. Ostuni, V. Piccolo, I. Barozzi, S. Polletti, A. Termanini, S. Bonifacio, A. Curina, E. Prosperini, S. Ghisletti, G. Natoli, Latent enhancers activated by stimulation in differentiated cells. *Cell* **152**, 157–171 (2013).
9. S. Chen, J. Yang, Y. Wei, X. Wei, Epigenetic regulation of macrophages: From homeostasis maintenance to host defense. *Cell. Mol. Immunol.* **17**, 36–49 (2020).
10. M. G. Netea, L. A. B. Joosten, E. Latz, K. H. G. Mills, G. Natoli, H. G. Stunnenberg, L. A. J. O'Neill, R. J. Xavier, Trained immunity: A program of innate immune memory in health and disease. *Science* **352**, aaf1098 (2016).
11. A. Mayran, J. Drouin, Pioneer transcription factors shape the epigenetic landscape. *J. Biol. Chem.* **293**, 13795–13804 (2018).
12. M. U. Kaikkonen, N. J. Spann, S. Heinz, C. E. Romanoski, K. A. Allison, J. D. Stender, H. B. Chun, D. F. Tough, R. K. Prinjha, C. Benner, C. K. Glass, Remodeling of the enhancer landscape during macrophage activation is coupled to enhancer transcription. *Mol. Cell* **51**, 310–325 (2013).
13. F. Comoglio, M. Simonatto, S. Polletti, X. Liu, S. T. Smale, I. Barozzi, G. Natoli, Dissection of acute stimulus-inducible nucleosome remodeling in mammalian cells. *Genes Dev.* **33**, 1159–1174 (2019).
14. Q. J. Cheng, S. Ohta, K. M. Sheu, R. Spreafico, A. Adelaja, B. Taylor, A. Hoffmann, NF-κB dynamics determine the stimulus specificity of epigenomic reprogramming in macrophages. *Science* **372**, 1349–1353 (2021).
15. J. Kim, K. M. Sheu, Q. J. Cheng, A. Hoffmann, G. Enciso, Stochastic models of nucleosome dynamics reveal regulatory rules of stimulus-induced epigenome remodeling. *Cell Rep.* **40**, 111076 (2022).
16. A.-C. Feng, B. J. Thomas, P. K. Purbey, F. M. de Melo, X. Liu, A. E. Daly, F. Sun, J. H.-H. Lo, L. Cheng, M. F. Carey, P. O. Scumpia, S. T. Smale, The transcription factor NF-κB orchestrates nucleosome remodeling during the primary response to Toll-like receptor 4 signaling. *Immunity* **57**, 462–477.e9 (2024).
17. G.-N. Zhao, D.-S. Jiang, H. Li, Interferon regulatory factors: At the crossroads of immunity, metabolism, and disease. *Biochim. Biophys. Acta* **1852**, 365–378 (2015).
18. S. Schmid, M. Mordstein, G. Kochs, A. García-Sastre, B. R. tenOever, Transcription factor redundancy ensures induction of the antiviral state. *J. Biol. Chem.* **285**, 42013–42022 (2010).
19. D. R. Ourthiague, H. Birnbaum, N. Ortenlöf, J. D. Vargas, R. Wollman, A. Hoffmann, Limited specificity of IRF3 and ISGF3 in the transcriptional innate-immune response to double-stranded RNA. *J. Leukoc. Biol.* **98**, 119–128 (2015).
20. S. Ghisletti, I. Barozzi, F. Mietton, S. Polletti, F. De Santa, E. Venturini, L. Gregory, L. Lonie, A. Chew, C.-L. Wei, J. Ragoussis, G. Natoli, Identification and characterization of enhancers controlling the inflammatory gene expression program in macrophages. *Immunity* **32**, 317–328 (2010).
21. S. Heinz, C. Benner, N. Spann, E. Bertolino, Y. C. Lin, P. Laslo, J. X. Cheng, C. Murre, H. Singh, C. K. Glass, Simple combinations of lineage-determining transcription factors prime cis-regulatory elements required for macrophage and B cell identities. *Mol. Cell* **38**, 576–589 (2010).
22. A.-J. Tong, X. Liu, B. J. Thomas, M. M. Lissner, M. R. Baker, M. D. Senagolage, A. L. Allred, G. D. Barish, S. T. Smale, A stringent systems approach uncovers gene-specific mechanisms regulating inflammation. *Cell* **165**, 165–179 (2016).
23. E. Platanitis, D. Demiroz, A. Schneller, K. Fischer, C. Capelle, M. Hartl, T. Gossenreiter, M. Müller, M. Novatchkova, T. Decker, A molecular switch from STAT2-IRF9 to ISGF3 underlies interferon-induced gene transcription. *Nat. Commun.* **10**, 2921 (2019).
24. S. Sakaguchi, H. Negishi, M. Asagiri, C. Nakajima, T. Mizutani, A. Takaoka, K. Honda, T. Taniguchi, Essential role of IRF-3 in lipopolysaccharide-induced interferon-β gene expression and endotoxin shock. *Biochem. Biophys. Res. Commun.* **306**, 860–866 (2003).
25. M. Abou El Hassan, K. Huang, M. B. K. Eswara, Z. Xu, T. Yu, A. Aubry, Z. Ni, I. Livne-bar, M. Sangwan, M. Ahmad, R. Bremner, Properties of STAT1 and IRF1 enhancers and the influence of SNPs. *BMC Mol. Biol.* **18**, 6 (2017).
26. K. Kang, M. Bachu, S. H. Park, K. Kang, S. Bae, K.-H. Park-Min, L. B. Ivashkiv, IFN-γ selectively suppresses a subset of TLR4-activated genes and enhancers to potentiate macrophage activation. *Nat. Commun.* **10**, 3320 (2019).
27. M. Csumita, A. Csermely, A. Horvath, G. Nagy, F. Monori, L. Göczi, H.-A. Orbea, W. Reith, L. Széles, Specific enhancer selection by IRF3, IRF5 and IRF9 is determined by ISRE half-sites, 5′ and 3′ flanking bases, collaborating transcription factors and the chromatin environment in a combinatorial fashion. *Nucleic Acids Res.* **48**, 589–604 (2020).
28. A. Mancino, A. Termanini, I. Barozzi, S. Ghisletti, R. Ostuni, E. Prosperini, K. Ozato, G. Natoli, A dual cis-regulatory code links IRF8 to constitutive and inducible gene expression in macrophages. *Genes Dev.* **29**, 394–408 (2015).
29. E. Platanitis, S. Gruener, A. Ravi Sundar Jose Geetha, L. Boccuni, A. Vogt, M. Novatchkova, A. Sommer, I. Barozzi, M. Müller, T. Decker, Interferons reshape the 3D conformation and accessibility of macrophage chromatin. *iScience* **25**, 103840 (2022).
30. D. Langlais, L. B. Barreiro, P. Gros, The macrophage IRF8/IRF1 regulome is required for protection against infections and is associated with chronic inflammation. *J. Exp. Med.* **213**, 585–603 (2016).
31. S.-L. Ng, B. A. Friedman, S. Schmid, J. Gertz, R. M. Myers, B. R. tenOever, T. Maniatis, IκB kinase ε (IKKε) regulates the balance between type I and type II interferon responses. *Proc. Natl. Acad. Sci. U.S.A.* **108**, 21170–21175 (2011).
32. M. Chatterjee-Kishore, K. L. Wright, J. P.-Y. Ting, G. R. Stark, How Stat1 mediates constitutive gene expression: A complex of unphosphorylated Stat1 and IRF1 supports transcription of the LMP2 gene. *EMBO J.* **19**, 4111–4122 (2000).
33. Y. Hu, K.-H. Park-Min, A. Yarilina, L. B. Ivashkiv, Regulation of STAT pathways and IRF1 during human dendritic cell maturation by TNF-α and PGE2. *J. Leukoc. Biol.* **84**, 1353–1360 (2008).
34. Y. Qiao, E. G. Giannopoulou, C. H. Chan, S. Park, S. Gong, J. Chen, X. Hu, O. Elemento, L. B. Ivashkiv, Synergistic activation of inflammatory cytokine genes by interferon-γ-induced chromatin remodeling and toll-like receptor signaling. *Immunity* **39**, 454–469 (2013).
35. S. L. Foster, D. C. Hargreaves, R. Medzhitov, Gene-specific control of inflammation by TLR-induced chromatin modifications. *Nature* **447**, 972–978 (2007).
36. C. S. Cheng, M. S. Behar, G. W. Suryawanshi, K. E. Feldman, R. Spreafico, A. Hoffmann, Iterative modeling reveals evidence of sequential transcriptional control mechanisms. *Cell Syst.* **4**, 330–343.E5 (2017).
37. Z. Ni, M. A. E. Hassan, Z. Xu, T. Yu, R. Bremner, The chromatin-remodeling enzyme BRG1 coordinates CIITA induction through many interdependent distal enhancers. *Nat. Immunol.* **9**, 785–793 (2008).
38. C. R. Escalante, J. Yie, D. Thanos, A. K. Aggarwal, Structure of IRF-1 with bound DNA reveals determinants of interferon regulation. *Nature* **391**, 103–106 (1998).
39. J. J. Zhang, U. Vinkemeier, W. Gu, D. Chakravarti, C. M. Horvath, J. E. Darnell Jr., Two contact regions between Stat1 and CBP/p300 in interferon γ signaling. *Proc. Natl. Acad. Sci. U.S.A.* **93**, 15092–15096 (1996).
40. Z. Ni, E. Karaskov, T. Yu, S. M. Callaghan, S. Der, D. S. Park, Z. Xu, S. G. Pattenden, R. Bremner, Apical role for BRG1 in cytokine-induced promoter assembly. *Proc. Natl. Acad. Sci. U.S.A.* **102**, 14611–14616 (2005).
41. S. Mitchell, E. L. Mercado, A. Adelaja, J. Q. Ho, Q. J. Cheng, G. Ghosh, A. Hoffmann, An NFκB activity calculator to delineate signaling crosstalk: Type I and II interferons enhance NFκB via distinct mechanisms. *Front. Immunol.* **10**, 1425 (2019).
42. S. Luecke, K. M. Sheu, A. Hoffmann, Stimulus-specific responses in innate immunity: Multilayered regulatory circuits. *Immunity* **54**, 1915–1932 (2021).
43. A. Hoffmann, Immune response signaling: Combinatorial and dynamic control. *Trends Immunol.* **37**, 570–572 (2016).
44. S. Luecke, A. Adelaja, X. Guo, S. Sen, R. Spreafico, A. Singh, Y. Liu, B. Taylor, J. Diaz, Q. Cheng, A. Hoffmann, Tonic TNF conditioning of macrophages safeguards stimulus-specific inflammatory responses. *EMBO Rep.* **24**, e55986 (2023).
45. C. L. Wilder, D. Lefaudeux, R. Mathenge, K. Kishimoto, A. Zuniga Munoz, M. A. Nguyen, A. S. Meyer, Q. J. Cheng, A. Hoffmann, A stimulus-contingent positive feedback loop enables IFN-β dose-dependent activation of pro-inflammatory genes. *Mol. Syst. Biol.* **19**, e11294 (2023).
46. Y. Zhang, T. Liu, C. A. Meyer, J. Eeckhoute, D. S. Johnson, B. E. Bernstein, C. Nusbaum, R. M. Myers, M. Brown, W. Li, X. S. Liu, Model-based analysis of ChIP-Seq (MACS). *Genome Biol.* **9**, R137 (2008).
47. F. Ramírez, D. P. Ryan, B. Grüning, V. Bhardwaj, F. Kilpert, A. S. Richter, S. Heyne, F. Dündar, T. Manke, deepTools2: A next generation web server for deep-sequencing data analysis. *Nucleic Acids Res.* **44**, W160–W165 (2016).
48. M. D. Robinson, D. J. McCarthy, G. K. Smyth, edgeR: A Bioconductor package for differential expression analysis of digital gene expression data. *Bioinformatics* **26**, 139–140 (2010).
49. A. R. Quinlan, I. M. Hall, BEDTools: A flexible suite of utilities for comparing genomic features. *Bioinformatics* **26**, 841–842 (2010).
50. H. S. Kaya-Okur, D. H. Janssens, J. G. Henikoff, K. Ahmad, S. Henikoff, Efficient low-cost chromatin profiling with CUT&Tag. *Nat. Protoc.* **15**, 3264–3283 (2020).
51. A. Dobin, C. A. Davis, F. Schlesinger, J. Drenkow, C. Zaleski, S. Jha, P. Batut, M. Chaisson, T. R. Gingeras, STAR: Ultrafast universal RNA-seq aligner. *Bioinformatics* **29**, 15–21 (2013).

**Acknowledgments:** We thank S. Smale for making ATAC-seq data from IRF3-deficient cells available in advance of publication. We acknowledge the expert evaluation of our statistical analyses by S. Park, assistant adjunct professor in mathematics and biostatistics at UCLA, supported by the QCBio Collaboratory Program. We acknowledge expert services by UCLA's Technology Center for Genomics and Bioinformatics (TCGB) and the Division of Laboratory Animal Medicine (DLAM). We thank all lab members for insightful discussions and A. Schiffman for critical reading of the manuscript. **Funding:** This project was supported by funds to A.H. (R01AI132835) and Q.J.C. (K08AI168567). C.C. was supported by the UCLA Microbial Pathogenesis Training Grant (T32AI007323). A.M. was supported by the UCLA URSP Hilton Endowment Scholarship. A.G. was supported by the UCLA Addressing Evolving Infectious Threats Training Grant (T32AI177290) and the Specialty Training and Advanced Research (STAR) program of the UCLA Department of Medicine. **Author contributions:** C.C., Q.J.C., and A.H. conceived and designed the study. C.C. performed most of the experiments. K.L. contributed experimental work. C.C. analyzed all of the data with assistance from A.M. A.G. and S.B. contributed human macrophage experiments and analysis. C.C. wrote the manuscript with contributions from Q.J.C. and A.H. All authors discussed the results and commented on the manuscript. **Competing interests:** The authors declare that they have no competing interests. **Data and materials availability:** All data needed to evaluate the conclusions in the paper are present in the paper or Supplementary Materials. All epigenomic profiling data reported in this manuscript have been deposited to GEO and are publicly available: GSE241821 for mouse and GSE270507 for human.

Submitted 27 February 2024
Accepted 4 December 2024
Published 7 January 2025
10.1126/scisignal.ado8860